Redox-Active Metal–Organic Composites for Highly Selective Oxygen Separation Applications

*Wen Zhang, Debasis Banerjee, Jian Liu, Herbert T. Schaef, Jarrod V. Crum, Carlos A. Fernandez, Ravi K. Kukkadapu, Zimin Nie, Satish K. Nune, Radha K. Motkuri, Karena W. Chapman, Mark H. Engelhard, James C. Hayes, Kurt L. Silvers, Rajamani Krishna, B. Peter McGrail, Jun Liu, and Praveen K. Thallapally**

Oxygen is widely used in today's energy conversion processes and in production of a variety of commodity materials and chemicals—a greater than $100 billion per year industry.[1,2] The current process technologies are geared to produce either purified oxygen or purified nitrogen from air by an energy-intensive cryogenic distillation process. Purified oxygen is required for a wide variety of applications that include portable adsorption units for medical applications and in space vehicles.[1] In addition, a large number of important energy technologies depend on O_2 production with low energy consumption and capital costs, such as oxy-fuel for CO_2 emission control, natural gas conversion, and gasification of biomass.[3] The energy- and capital-intensive cryogenic separation process used in large-scale production of oxygen is prohibitively expensive for many small-scale renewable applications.[2] On the other hand, oxygen removal is necessary to improve the shelf-life of various foods and beverages due to oxidative food spoiling reactions. Even after flushing a food package with an inert gas, the amount of residual oxygen in a package headspace is still significant (2%), due to the ability of the food to trap air. Therefore, there is an urgent need for alternative technologies and novel materials for energy- and cost-efficient oxygen separation from air. Zeolite molecular sieves have been used for O_2 adsorption and separation,[4] but still fall short compared to recently reported solid state adsorbents based on high surface area, crystalline metal–organic frameworks (MOFs).[5–7] In this regard, selective adsorption of O_2 from N_2 using M^{2+} based MOFs—$M_3(btc)_2$ (M = Cr, Fe; btc[3] = 1,3,5-benzenetricarboxylate) and MOF-74 Fe—are shown to exhibit steep O_2-adsorption isotherms at room temperature (RT).[5] However, these MOFs are not stable in air because of presence of exposed M^{2+} species, which readily oxidizes to form M^{3+} in presence of oxygen.[6,8] In light of these underlying challenges, a system where a redox-active M^{2+} species can be generated within a porous framework is expected to be significantly more air stable because of the pore-confinement effect.[9]

Herein, we present a strategy to improve O_2-adsorption and O_2/air-separation selectivity at room temperature using a composite material, where a redox-active organometallic molecule, ferrocene, was used as a precursor to form O_2-selective Fe^{2+} species within a thermochemically stable, highly porous MOF, MIL-101 [MIL = Materials from Institut Lavoisier]. This strategy is in direct contrast to previously reported O_2.selective MOF-based materials, which possess accessible open M^{2+} metal sites on the pore surface.[5,6] The advantages of our method include the absence of superoxide formation within the host framework as a result of high framework stability. Ferrocene [$Fe(\eta^5\text{-}C_5H_5)_2$] (Fc) was chosen as a suitable oxygen scavenger for two reasons: i) it contains π-electron-rich ligands and is expected to interact with the more electron-deficient phenyl rings of the host framework through π–π donor–acceptor interactions, and ii) Fc is a redox-active organometallic compound with an Fe^{2+}oxidation state, which can then converted in situ to accessible, redox-active Fe(II) species within the MOF pore space.[6] MIL-101(Cr) was selected as the host matrix because of the relative ease of preparing high-quality material with high surface area and its micro- and mesoporous cage structure. MIL-101 was synthesized using a reported procedure and characterized using powder X-ray diffraction (PXRD) and Brunauer–Emmett–Teller surface-area analysis (Figure S1 and S2, Supporting Information).[10] MIL-101 consists of two cage windows with internal diameters of ≈29 and 34 Å, which in

Dr. W. Zhang, Dr. D. Banerjee,
H. T. Schaef, Dr. P. K. Thallapally
Physical & Computational Sciences Directorate
Pacific Northwest National Laboratory
Richland, WA 99352, USA
E-mail: Praveen.thallapally@pnnl.gov
Dr. J. Liu, J. V. Crum, Dr. C. A. Fernandez,
Dr. Z. Nie, Dr. S. K. Nune, Dr. R. K. Motkuri,
Dr. B. P. McGrail, Dr. J. Liu
Energy and Environment Directorate
Pacific Northwest National Laboratory
Richland, WA 99354, USA
Dr. R. K. Kukkadapu, Dr. M. H. Engelhard
Environmental Molecular Sciences Laboratory
Pacific Northwest National Laboratory
Richland, WA 99354, USA
Dr. K. W. Chapman
X-ray Science Division
Advanced Photon Source
Argonne National Laboratory
Argonne, IL 60439, USA
Dr. J. C. Hayes, Dr. K. L. Silvers
National Security Directorate
Pacific Northwest National Laboratory
Richland, WA 99352, USA
Prof. R. Krishna
Van't Hoff Institute for Molecular Sciences
University of Amsterdam
Science Park 904, 1098 XH, Amsterdam, The Netherlands

DOI: 10.1002/adma.201600259

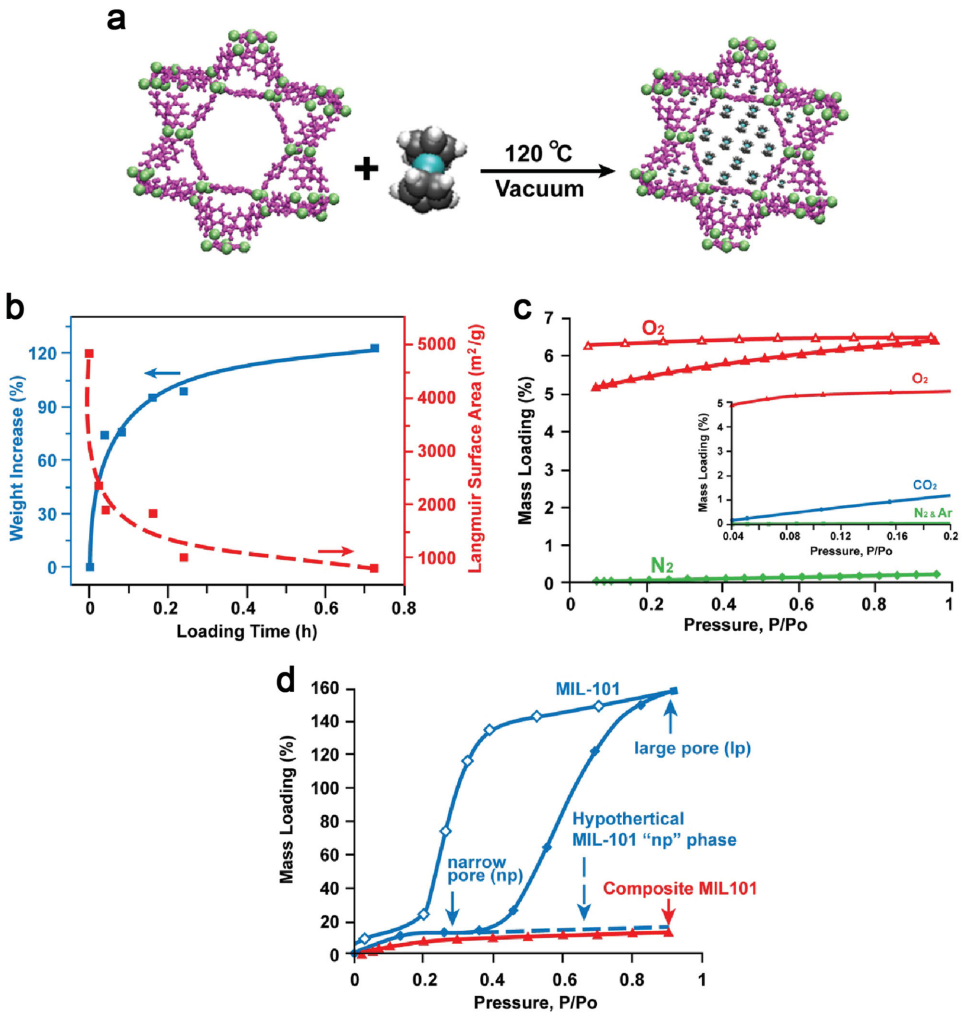

Figure 1. Redox-active metal–organic composite. a) Vapor deposition of Fc inside the porous framework (MIL-101). b) Increase in weight (blue) and decrease in surface area (red) as a function of Fc loading. c) Adsorption of O_2; negligible adsorption capacity toward N_2, CO_2, and Ar at RT. d) RT water adsorption in MIL-101 and composite MIL-101.

turn correspond to accessible pore volumes of ≈12 700 and ≈20 600 Å^3, respectively.[11] The MIL-101 can accommodate up to ≈45 and ≈70 molecules of Fc in the smaller and larger cages, respectively, assuming the molecular volume of Fc is 280 Å^3 (**Figure 1**a). The pore-size distribution analysis (Horváth–Kawazoe method) on as-synthesized MIL-101 confirmed the presence of two distinct pores (of width 25 and 35 Å) with a pore volume of 1.6 cc g^{-1}. The Fc was loaded in heated MIL-101 by a vapor-deposition technique at 120 °C under vacuum as a function of time (Figure S3, Supporting Information). Such techniques have been reported by others in the literature, more prominently by Fischer and co-workers.[12,13] The surface area of the MIL-101 (4800 m^2 g^{-1}) decreased as the amount of Fc increased (Figure 1b). Similarly, the weight of the MIL-101 increased gradually and reached a maximum at ≈72 h. The calculated loading of Fc after 72 h was 1.2 g of Fc per gram of MIL-101 (4.5 Fc per formula unit). The Fc-loaded MIL-101 (after 72 h) [hereafter termed Fc@MIL-101] showed an expected decrease in pore volume to 0.25 cc g^{-1} and a surface area of ≈1000 m^2 g^{-1}, which is still very high compared to many MOFs, zeolites, and porous carbon materials reported thus far (Figure S4 and S5, Supporting Information). Along with reduction of surface area and pore volume, the color of MIL-101 changes from green to black as a function of Fc loading, confirming the proposed charge-transfer interactions between the host/guest and successful loading of Fc into the crystal lattice (Figure S6, Supporting Information).

Thermogravimetric analysis of MIL-101 has four main weight-loss steps, which correspond to the removal of the adsorbed water molecules followed by decomposition of the framework at ≈350 °C (Figure S7, Supporting Information). Interestingly, desorption of the included Fc in activated MIL-101 did not occur upon heating until 200 °C, significantly higher than the sublimation temperature of the pure Fc material (Figure S8, Supporting Information). The higher desorption temperature is probably due to the stronger interactions between the electron-rich and electron-deficient host–guest species; similar observations have been made in MOFs and other classes of materials.[13,14] The PXRD experiments suggest the Fc@MIL-101 diffraction pattern is very similar to that

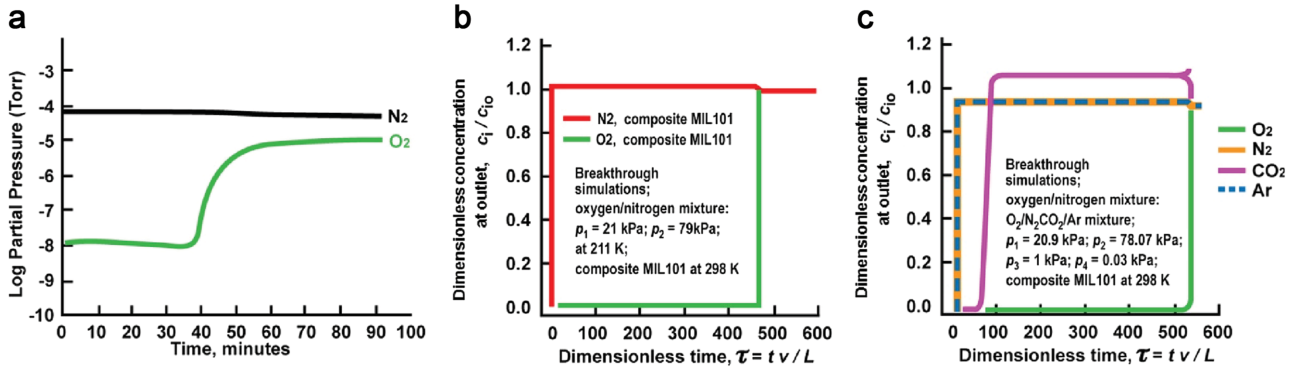

Figure 2. Separation of O_2 from air using redox-active composite MIL-101. a) Experimental breakthrough characteristics using feed of 21% O_2 and 79% N_2. b) Simulated breakthrough using feed of 21% O_2 and 79% N_2. c) Separation of O_2 from breathing air consisting of 70% N_2, 20% O_2, 1% Ar, and 0.09% CO_2.

of MIL-101 except that the intensity of some diffraction peaks changes considerably (Figure S9, Supporting Information).

The adsorption experiments at RT suggest the Fc@MIL-101 does not have any affinity toward oxygen. Therefore Fc@MIL-101 was heated at a higher temperature (200 °C) to remove any Fc strongly adhered to the surface. At 1 bar, the Fc@MIL-101 heated at 200 °C showed an enhanced oxygen uptake (10 cc g^{-1}) with hysteresis in the desorption profile. This observation led us to investigate the oxygen-adsorption profile for Fc@MIL-101 as a function of heating temperature. The Fc@MIL-101 heated at 350 °C for 12 h (hereafter composite MIL-101) has 4× and 40× higher adsorption capacity (6.5 wt% or 45 cc g^{-1}) at RT, with respect to the same material heated at 200 °C and at RT (Figure S10, Supporting Information). The desorption profile shows significant hysteresis, indicating stronger interactions between the adsorbed oxygen and the composite-MIL-101. Under similar conditions, MIL-101 without Fc (heated at 350 °C) adsorbed 12 cc g^{-1} of oxygen (Figure S11, Supporting Information), indicating the importance of Fc loading and subsequent heating for enhanced O_2 adsorption. Single-component gas-adsorption experiments (N_2, Ar, CO_2, H_2O) performed on the composite material at RT revealed that it adsorbs very small quantities of N_2 (≈2 cc g^{-1}), Ar (3 cc g^{-1}), and CO_2 (20 cc g^{-1}) (Figure 1c and Figure S12, Supporting Information). The composite MIL-101 adsorbs 12 wt% of water at relative humidity of 100% compared to MIL-101 (160 wt%). The water-adsorption profile of the composite MIL-101 is identical to the hypothetical narrow pore phase of MIL-101 (Figure 1d and Figure S12, Supporting Information). This suggests that, upon heating (350 °C), the composite MIL-101 material is transformed to the hypothetical narrow pore phase with significant porosity (Langmuir surface area: 424 m^2 g^{-1}; Table S1, Supporting Information).

Based on these findings, we further explored the capability of this composite material for real-world air-separation applications using a custom built breakthrough reactor coupled with a residual-gas analyzer (Figure S13, Supporting Information). The column packed with composite material was fed with an N_2/O_2 gas (21% O_2 and 79% N_2 by volume) mixture. The nitrogen broke through the column immediately after injection (<1 min), while oxygen broke through after ≈40 min. These results clearly indicate that the material is exceptionally selective toward oxygen over nitrogen (**Figure 2**a). The composite has an excellent selectivity for O_2/N_2 separation, since N_2 is virtually excluded from the pores of the material. Breakthrough experiments were conducted using breathing air with a composition of 70% N_2, 20% O_2, 1% Ar, and 0.09% CO_2; however, we were unable to detect the low concentrations of CO_2 and Ar using our experimental setup because the concentrations were below the detection limit. Therefore simulated breakthrough experiments were performed for ambient air using pure-component adsorption-isotherm data (Figure 2b,c, and Figure S14–S19 and Table S2, Supporting Information).[15] The O_2/N_2-adsorption selectivity was found to be about three to six orders of magnitude higher than that obtained with MOF 74 Fe (Figure S16 and S17, Supporting Information).[6] Transient breakthrough simulations indicate the composite material has a higher productivity of pure N_2 compared to the leading MOF (MOF-74 Fe) material. This could be due to the higher selectivity overcoming the capacity disadvantage with respect to MOF-74 Fe. These

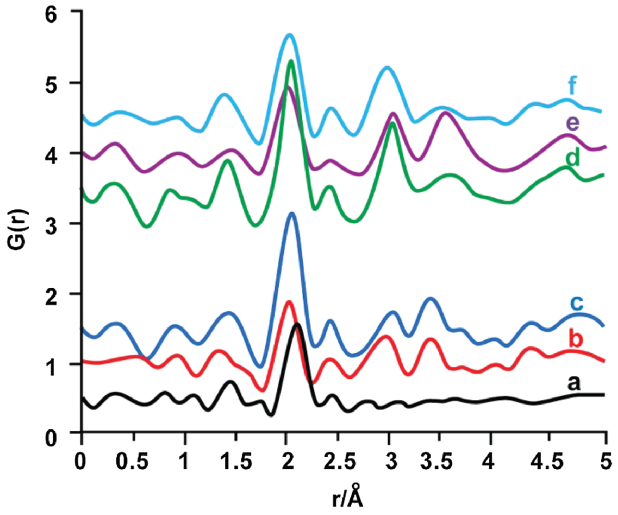

Figure 3. Pair distribution function analysis. $G(r)$ were obtained from the total scattering data: a) Fc, b) MIL-101, c) differential PDF analysis of Fc@MIL-101, d) composite MIL-101, e) composite exposed to O_2, and f) MIL-101 heated at 350 °C.

results demonstrate that the separation of O_2 from breathing air is feasible.

To understand the structural stability, PXRD experiments were conducted on MIL-101 (heated at 350 °C) and composite MIL-101. Both materials lose long-range order after heating, as exhibited by the PXRD pattern (Figure S20, Supporting Information). However, energy-dispersive X-ray (EDX) spectroscopy and elemental-mapping analysis on MIL-101 show the uniform distribution of elemental chromium, oxygen, and carbon (Figure S21, Supporting Information). Similarly, EDX studies on composite MIL-101 results clearly indicate the presence of Fe along with Cr, O, and C at all temperatures (Figure S22 and S23, Supporting Information). This observation further supports the presence of iron species embedded in the host framework, even after the sample was heated at 350 °C. A decrease in Cr and increase in Fe concentration were observed at the surface of composite MIL-101, which is attributed to the possible leaching of iron species out of the pores of MIL-101 (Table S3, Supporting Information).

In order to probe the local structural information independent of crystallinity as a weighted histogram of all atom–atom distances within the composite, pair distribution function (PDF) analysis using high-energy X-ray scattering data were performed on Fc, MIL-101, and Fc@MIL-101 heated at variable temperatures and subsequently exposed to oxygen (Figure S24, Supporting Information).[16] From the PDF data, well-defined peaks were evident below ≈6 Å for MIL-101 that correspond to Cr–O cluster coordination and the 1,2 and 1,3 distances in the bdc (bdc = terephthalate) ligand. Despite the crystalline nature of MIL-101, well-defined individual atom–atom features were not readily apparent in the PDF at longer distances due to overlap between features of similar distance. The PDF of pure Fc is dominated by a sharp peak at 2.060 Å corresponding to the Fe–C distance. In contrast, differential PDF analysis of Fc@MIL-101 shows that these features from the Fc are retained (**Figure 3**). The PDF analysis on O_2-exposed composite MIL-101 shows that it possesses local structure motifs similar to those found in MIL-101 along with a crystalline component, structurally similar to a ferritic spinel phase, with nanoscale domains or particles of ≈4 nm (Figure S25, Supporting Information). The refined lattice parameter, a = 8.346(22) Å (over the r range 15–30 Å), suggests it is of maghemite (γ-Fe_2O_3, a = 8.33 Å) with Fe^{2+} vacancies. The PDF for the O_2-sorbed composite is not well modeled to any known chromium oxide phases; instead, the results are more consistent with the local structural motifs found in MIL-101 with reduced porosity embedded with maghemite (Fe_2O_3) nanoclusters. The absence of Fc peaks in the PDF data clearly demonstrated that almost all Fc within the MOF is converted to the Fe^{2+} species under our experimental conditions.

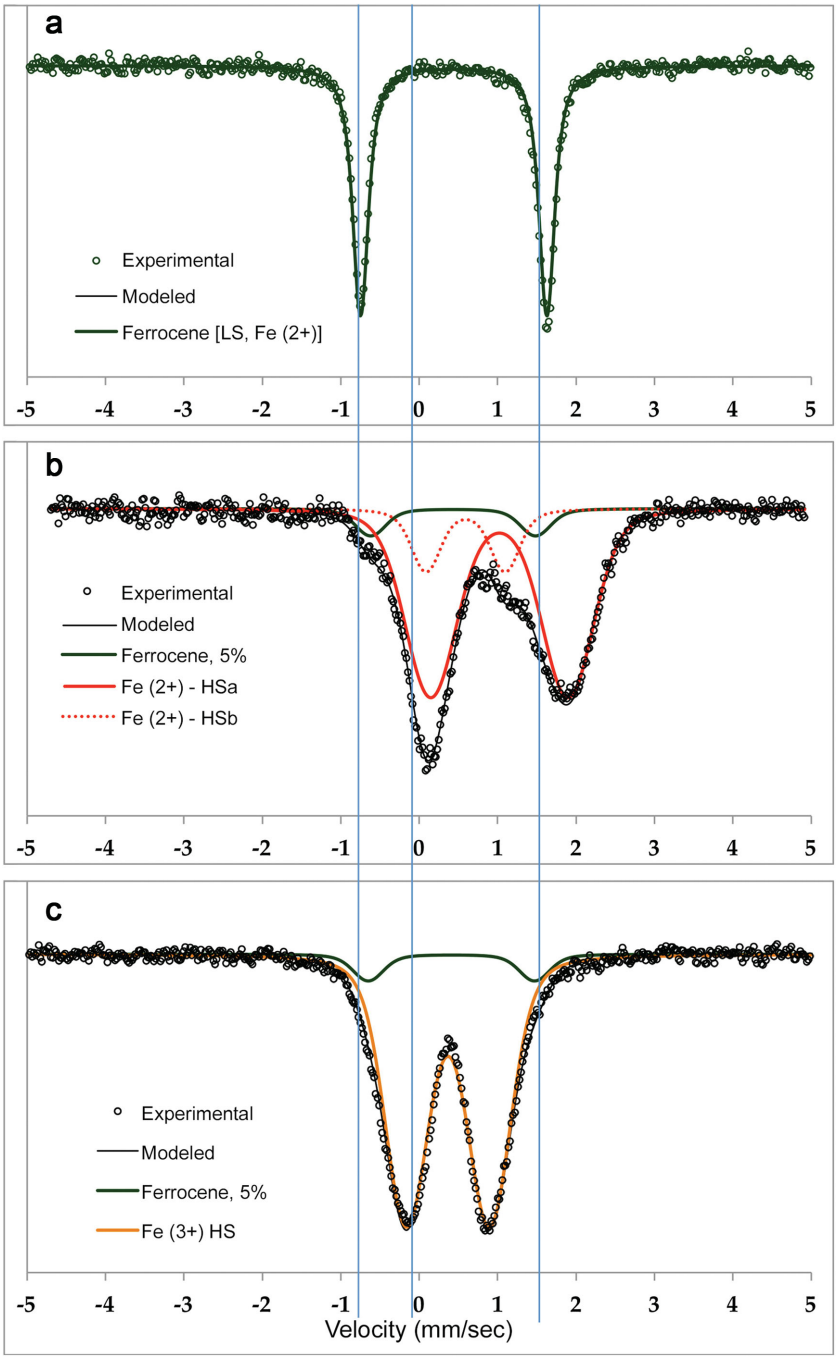

Figure 4. Mössbauer spectroscopy at RT. a) Pristine Fc (top), b) composite MIL-101 (middle) in anaerobic conditions, and c) composite MIL-101 after O_2 adsorption (bottom).

To further support PDF observations, X-ray photoelectron spectroscopy (XPS) of the composite material before (anaerobic conditions) and after exposure to O_2 suggests that the

oxidation state of Fe changes from 2+ to 3+; however, no change was observed in the Cr oxidation state (Figure S26, Supporting Information). This was reflected in the Fe $2p_{3/2}$ peak position at 710 eV (Fe^{2+}) in an anaerobic sample, compared to 715 eV for a sample exposed to oxygen (Fe^{3+}). Similarly, Mössbauer spectroscopy measurements (a ^{57}Fe-specific technique) were obtained on Fc (**Figure 4**a), and composite MIL-101 both before and after exposure to oxygen (Figure 4b,c**)**. The derived Mössbauer spectral parameters of Fc indicate a low-spin Fe^{2+} (S = 0; diamagnetic), which is in good agreement with the reported literature values (Table S4, Supporting Information). The Mössbauer spectrum of the composite heated at 350 °C (anaerobic) is rather complex: two Fe^{2+} doublets (high spin in nature; S = 2; paramagnetic; red traces in Figure 4b) and some residual Fc (≈5% of the total Fe). The transformation of low-spin Fe^{2+} to high-spin Fe^{2+} suggests significant modification of the Fc environment. On the other hand, two high-spin Fe^{2+} doublets and the broadness of the peaks imply the presence of multiple Fe sites with somewhat similar local environments, which may be due to localization of Fe in different pores or their existence on different surfaces. Both of the high-spin Fe^{2+} doublets more or less transformed to a high-spin Fe^{3+} (S = 5/2) moiety upon exposure to oxygen (Figure 4c). The center shift of high-spin Fe^{3+} is typical for nanoparticles of Fe^{3+}-oxide, and its relatively higher quadrupole splitting than pure Fe-oxide(s) suggests that sizeable Fe environments of the phase are significantly distorted. Furthermore, the absence of Fe^{2+} suggests the composite material is free of large-particle Fe^{2+}-containing oxides, such as $FeCrO_4$ or magnetite/maghemite. From PDF and Mössbauer results, the final composite is most likely a maghemite (γ-Fe_2O_3, a pure Fe^{3+} mineral) within the reduced form of MIL-101. The absence of sextet features typical of (nano)maghemite in its 77 K spectrum (Figure S27, Supporting Information), however, suggests it to be maghemite that is intimately associated with composite material. In order to know the cycle stability of the composite, experiments were performed at room temperature by activating at 350 °C after each adsorption cycle. The composite shows the reduced O_2 capacity, this can be explained by the presence of reduced amount of Fe^{2+} nanoclusters after each cycle due to the formation of maghemite (Figure S28, Supporting Information). This is in line with the commercially used O_2 absorber such as AGELESS and MOFs exposed with M^{2+} sites where these sorbents have no cycle stability due to the chemical reaction between the sorbent and oxygen.[6,8]

The redox-active composite material with the exceptional capacity and high selectivity for oxygen demonstrated here would be far less energy intensive than cryogenic distillation, potentially making these composites useful for oxygen-separation and sensing applications. The selective adsorption of O_2 from relevant gas mixtures as shown by experimental and simulated breakthrough experiments would have significant practical applications and offer improvements over current air-separation technologies. Our results demonstrate a proof of concept for oxygen separation using redox-active composite materials that are derived from high-surface-area materials incorporated with redox-active organometallic building blocks as an Fe^{2+} precursor.[17] Furthermore, we probed the mechanism and transformation of low-spin Fc (Fe^{2+}) to maghemite (an Fe^{3+} mineral) within the porous framework by combination of Mössbauer spectroscopy and PDF analysis.

Experimental Section

MIL-101 was synthesized using a reported procedure.[10] The as-synthesized material was heated followed by Fc loading at 110 °C under vacuum. The detailed synthesis procedure of MIL-101 and Fc@MIL-101 is described below.

Preparation of MIL-101: In a typical experiment, terephthalic acid (H_2BDC, Aldrich, 98%, 1.66 g, 10 mmol) was added to an alkaline solution of tetramethylammonium hydroxide (Moses Lake Industries, Inc., 25% V/V, 50 mL, 0.05 mol L^{-1}) and stirred at RT for 10 min. Chromium (III) nitrate nonahydrate ($Cr(NO_3)_3{\cdot}9H_2O$, Sigma–Aldrich, 4.0 g, 10 mmol) was subsequently added to the mixture and stirred for 20 min. The resulting mixture was then transferred into a 125 mL Teflon-lined autoclave and heated at 180 °C for 24 h and then cooled to RT at a rate of 10 °C min^{-1}. The microcrystalline green powder was collected by repeated centrifugation and thorough washing with distilled water and exchanged in methanol (MeOH, 99%, Sigma–Aldrich) for two days. The product was then collected by centrifugation and dried at RT (yield: 3.389 g, 40% based on metal salt)

Preparation of Fc@MIL-101: In a typical experiment, a heated sample (150 °C per 24 h) of MIL-101 (50 mg, 1.785 mmol) was kept inside a 20 mL scintillation vial and was inserted into a 150 mL beaker containing 100 mg of Fc (ferrocene, Aldrich, 98%, 0.538 mmol). The beaker was covered with a watch glass and kept under vacuum in a vacuum oven at RT for 12 h, followed by heating at 120 °C for 72 h under vacuum in order to sublime the Fc. The product changed from brownish green to black. The surface-adsorbed Fc was removed from the black product by heating at 200 °C for 12 h.

Composite MIL-101: The composite MIL-101 was prepared by heating Fc@MIL-101 under dynamic vacuum (10^{-4} Torr) for 12 h at 350 °C. All the characterizations (XPS, EDX, PDF, and Mössbauer spectroscopy) and gas adsorption and column breakthrough and simulation breakthrough measurements were conducted on composite MIL-101 at room temperature unless otherwise mentioned.

Supporting Information

Supporting Information is available from the Wiley Online Library or from the author.

Acknowledgements

The authors would like to acknowledge the Office of Basic Energy Sciences (BES), U.S. Department of Energy (DOE), and DOE/BES/Division of Materials Sciences and Engineering (Award No. KC020105-FWP12152). A portion of this work (XPS and Mössbauer spectroscopy) was performed at Environmental Molecular Science Laboratory (EMSL), a national scientific user facility sponsored by the Department of Energy's Office of Biological and Environmental Research and located at Pacific Northwest National Laboratory (PNNL). PNNL is a multiprogram national laboratory operated for the U.S. Department of Energy by Battelle Memorial Institute under Contract No. DE-AC05-76RL01830. Work done at Argonne and use of the Advanced Photon Source, an Office of Science User Facility operated for the U.S. Department of Energy Office of Science by Argonne National Laboratory, were supported by the U.S. Department of Energy under Contract No. DE-AC02-06CH11357.

Received: January 15, 2016
Revised: February 2, 2016
Published online: March 8, 2016

[1] J. Ermsley, *Nature's Building Blocks: An A–Z Guide to the Elements*, Oxford University Press, New York **2001**.
[2] a) F. G. Kerry, *Industrial Gas Handbook: Gas Separation and Purification*, CRC Press, Boca Raton, FL, USA **2007**; b) N. N. Greenwoord, A. Earnshaw, *Chemistry of Elements*, Butterworth-Heinemann, Burlington, MA, USA **1997**.
[3] a) M. P. Aznar, M. A. Caballero, J. Gil, J. A. Martin, J. Corella, *Ind. Eng. Chem. Res.* **1998**, *37*, 2668; b) B. J. P. Buhre, L. K. Elliott, C. D. Sheng, R. P. Gupta, T. F. Wall, *Prog. Energy Combust. Sci.* **2005**, *31*, 283; c) K. Aasberg-Petersen, J. H. B. Hansen, T. S. Christensen, I. Dybkjaer, P. S. Christensen, C. S. Nielsen, S. E. L. W. Madsen, J. R. Rostrup-Nielsen, *Appl. Catal., A* **2001**, *221*, 379.
[4] M. Shi, J. Kim, J. A. Sawada, J. Lam, S. Sarabadan, T. M. Kuznicki, S. M. Kuznicki, *AICHE J.* **2013**, *59*, 982.
[5] a) L. J. Murray, M. Dinca, J. Yano, S. Chavan, S. Bordiga, C. M. Brown, J. R. Long, *J. Am. Chem. Soc.* **2010**, *132*, 7856; b) H. Farukawa, K. E. Cordova, M. O'Keeffe, O. M. Yaghi, *Science* **2013**, *341*, 974.
[6] E. D. Bloch, L. J. Murray, W. L. Queen, S. Chavan, S. N. Maximoff, J. P. Bigi, R. Krishna, V. K. Peterson, F. Grandjean, G. J. Long, B. Smit, S. Bordiga, C. M. Brown, J. R. Long, *J. Am. Chem. Soc.* **2011**, *133*, 14814.
[7] a) S. Kitagawa, R. Kitaura, S. Noro, *Angew. Chem. Int. Ed.* **2004**, *43*, 2334; b) G. Ferey, *Chem. Soc. Rev.* **2008**, *37*, 191; c) H.-C. Zhou, J. R. Long, O. M. Yaghi, *Chem. Rev.* **2012**, *112*, 673; d) J. B. DeCoste, M. H. Weston, P. E. Fuller, T. M. Tovar, G. W. Peterson, M. D. LeVan, O. K. Farha, *Angew. Chem. Int. Ed.* **2014**, *53*, 14092; e) R. K. Motkuri, H. V. R. Annapureddy, M. Vijaykumar, H. T. Schaef, P. F. Martin, B. P. McGrail, L. X. Dang, R. Krishna, P. K. Thallapally, *Nat. Commun.* **2014**, *5*, 4368; f) D. Banerjee, A. J. Cairns, J. Liu, R. K. Motkuri, S. K. Nune, C. A. Fernandez, R. Krishna, D. M. Strachan, P. K. Thallapally, *Acc. Chem. Res.* **2015**, *48*, 211.
[8] a) M. Anpo, M. Che, B. Fubini, E. Garrone, E. Giamello, M. C. Paganini, *Top. Catal.* **1999**, *8*, 189; b) S. N. Maximoff, B. Smit, *Nat. Commun.* **2014**, *5*, 4032.
[9] B. Nepal, S. Das, *Angew. Chem. Int. Ed.* **2013**, *52*, 7224.
[10] J. Yang, Q. Zhao, J. Li, J. Dong, *Microporous Mesoporous Mater.* **2010**, *130*, 174.
[11] G. Ferey, C. Mellot-Draznieks, C. Serre, F. Millange, J. Dutour, S. Surble, I. Margiolaki, *Science* **2005**, *309*, 2040.
[12] a) M. Meilikhov, K. Yusenko, R. A. Fischer, *J. Am. Chem. Soc.* **2009**, *131*, 9644; b) M. Meilikhov, K. Yusenko, R. A. Fischer, *Dalton Trans.* **2010**, *39*, 10990.
[13] M. Meilikhov, K. Yusenko, R. A. Fischer, *Dalton Trans.* **2009**, 600.
[14] J. L. Atwood, L. J. Barbour, A. Jerga, *Science* **2002**, *296*, 2367.
[15] a) R. Krishna, *Microporous Mesoporous Mater.* **2014**, *185*, 30; b) R. Krishna, J. R. Long, *J. Phys. Chem. C* **2011**, *115*, 12941.
[16] R. Harrington, D. B. Hausner, N. Bhandari, D. R. Strongin, K. W. Chapman, P. J. Chupas, D. S. Middlemiss, C. P. Grey, J. B. Parise, *Inorg. Chem.* **2010**, *49*, 325.
[17] a) J. An, O. K. Farha, J. T. Hupp, E. Pohl, J. I. Yeh, N. L. Rosi, *Nat. Commun.* **2012**, *3*, 604; b) T. Ben, H. Ren, S. Q. Ma, D. P. Cao, J. H. Lan, X. F. Jing, W. C. Wang, J. Xu, F. Deng, J. M. Simmons, S. L. Qiu, G. S. Zhu, *Angew. Chem. Int. Ed.* **2009**, *48*, 9457; c) S. H. Yang, J. L. Sun, A. J. Ramirez-Cuesta, S. K. Callear, W. I. F. David, D. P. Anderson, R. Newby, A. J. Blake, J. E. Parker, C. C. Tang, M. Schroder, *Nat. Chem.* **2012**, *4*, 887; d) J. Rabone, Y. F. Yue, S. Y. Chong, K. C. Stylianou, J. Bacsa, D. Bradshaw, G. R. Darling, N. G. Berry, Y. Z. Khimyak, A. Y. Ganin, P. Wiper, J. B. Claridge, M. J. Rosseinsky, *Science* **2010**, *329*, 1053; e) T. Tozawa, J. T. A. Jones, S. I. Swamy, S. Jiang, D. J. Adams, S. Shakespeare, R. Clowes, D. Bradshaw, T. Hasell, S. Y. Chong, C. Tang, S. Thompson, J. Parker, A. Trewin, J. Bacsa, A. M. Z. Slawin, A. Steiner, A. I. Cooper, *Nat. Mater.* **2009**, *8*, 973.

ADVANCED MATERIALS

Supporting Information

for *Adv. Mater.,* DOI: 10.1002/adma.201600259

Redox-Active Metal–Organic Composites for Highly Selective Oxygen Separation Applications

Wen Zhang, *Debasis Banerjee*, *Jian Liu*, *Herbert T. Schaef*, *Jarrod V. Crum*, *Carlos A. Fernandez*, *Ravi K. Kukkadapu*, *Zimin Nie*, *Satish K. Nune*, *Radha K. Motkuri*, *Karena W. Chapman*, *Mark H. Engelhard*, *James C. Hayes*, *Kurt L. Silvers*, *Rajamani Krishna*, *B. Peter McGrail*, *Jun Liu*, *and Praveen K. Thallapally**

Supplementary Information

Redox Active Metal Organic Composites for Highly Selective Oxygen Separation Applications

Wen Zhang [1], Debasis Banerjee [1], Jian Liu [2], Herbert T. Schaef [1], Jarrod V. Crum[2], Carlos A. Fernandez [2], Ravi Kukkadapu [3], Zimin Nie [2], Satish K. Nune [2], Radha K. Motkuri [2], Karena W. Chapman [4], M. H. Engelhard [3], James C. Hayes [5], Kurt L. Silvers [5], Rajamani Krishna [6], B. Peter McGrail [2], Jun Liu [2], Praveen K. Thallapally [1,*]

[1]Fundamental & Computational Sciences Directorate, Pacific Northwest National Laboratory, Richland, WA 99352, USA. [2]Energy and Environment Directorate, Pacific Northwest National Laboratory, Richland, WA 99352, USA. [3] Environmental Molecular Science Laboratory, Pacific Northwest National Laboratory, Richland, WA 99352, USA. [4]X-ray Science Division, Advanced Photon Source, Argonne National Laboratory, Argonne, IL, 60439 USA. [5]National Security Directorate, Pacific Northwest National Laboratory, Richland, WA 99352, USA. [6]Van 't Hoff Institute for Molecular Sciences, University of Amsterdam, Science Park 904, 1098 XH Amsterdam, The Netherlands. Correspondence and requests for materials should be addressed to P.K.T (email: praveen.thallapally@pnnl.gov)

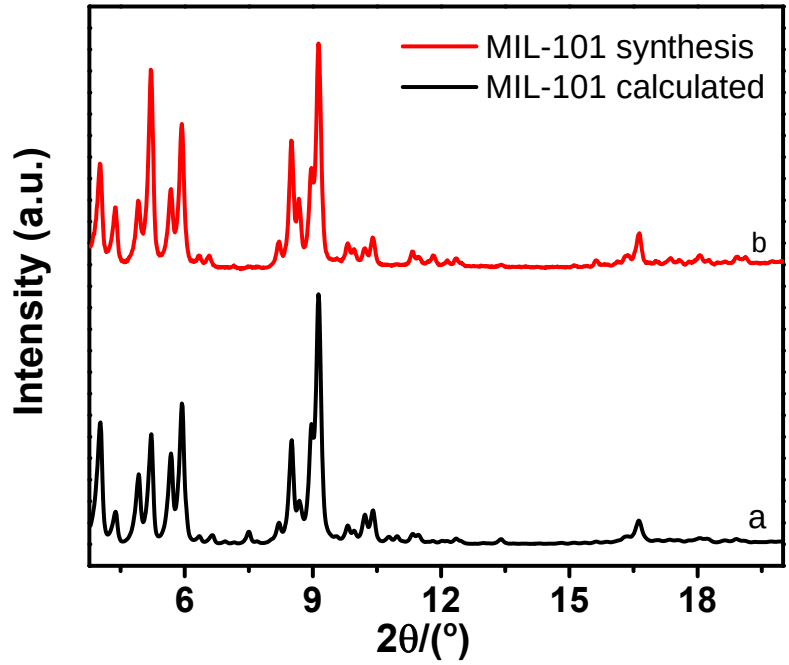

Figure S1. PXRD for (a) simulated MIL-101 and (b) synthesized MIL-101.

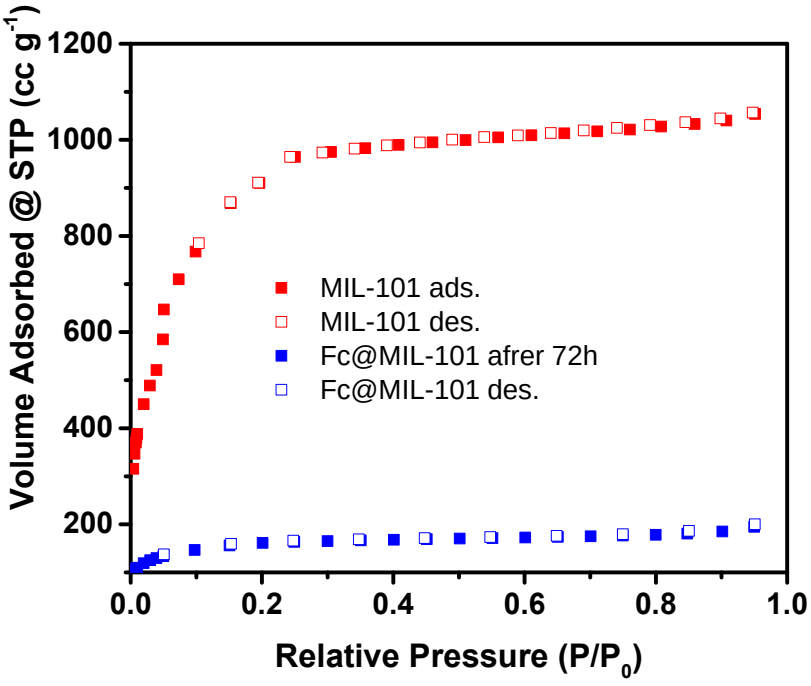

Figure S2. N_2 sorption isotherm collected at 77K and 1 atm pressure for MIL-101 and Fc@MIL-101 (72h, degas 200°C, 12h).

Ferrocene decomposition: Experiments were conducted to decompose the pristine ferrocene at 350 C (same temperature as composite) but leaches out of the column due to highly volatile nature of the ferrocene as shown below

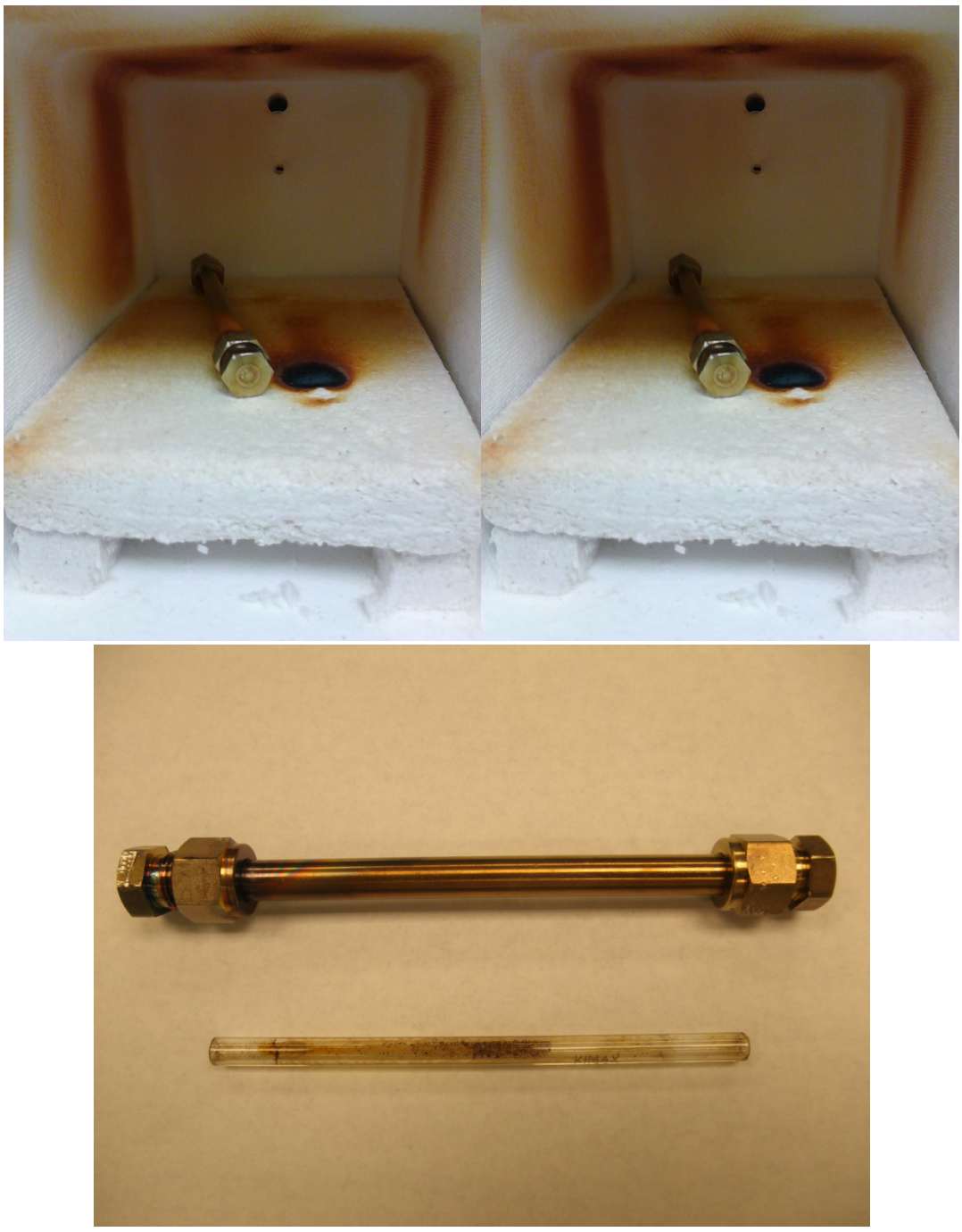

Figure. S3. Ferrocene leaches out of the column

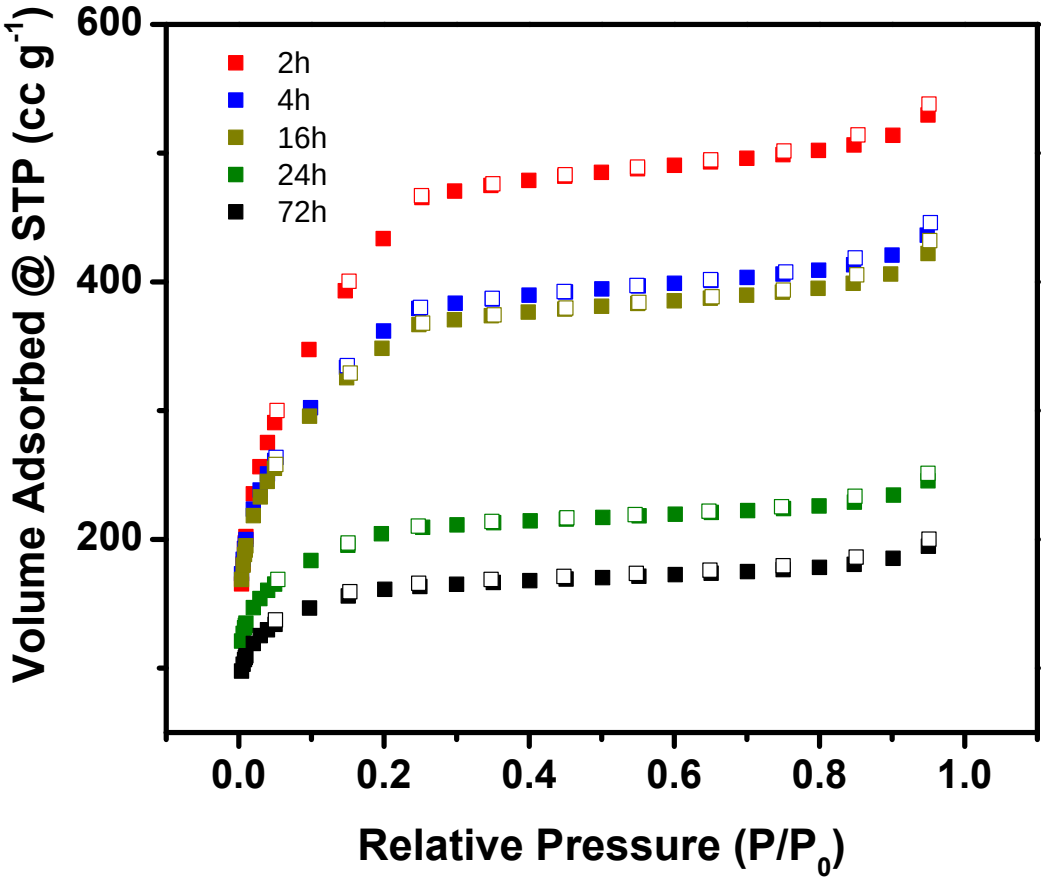

Figure S4. Nitrogen Adsorption-desorption Isotherms at 77K for Fc@MIL-101(without heating) as a function of different loading time (open symbol-desorption, closed symbol: adsorption)

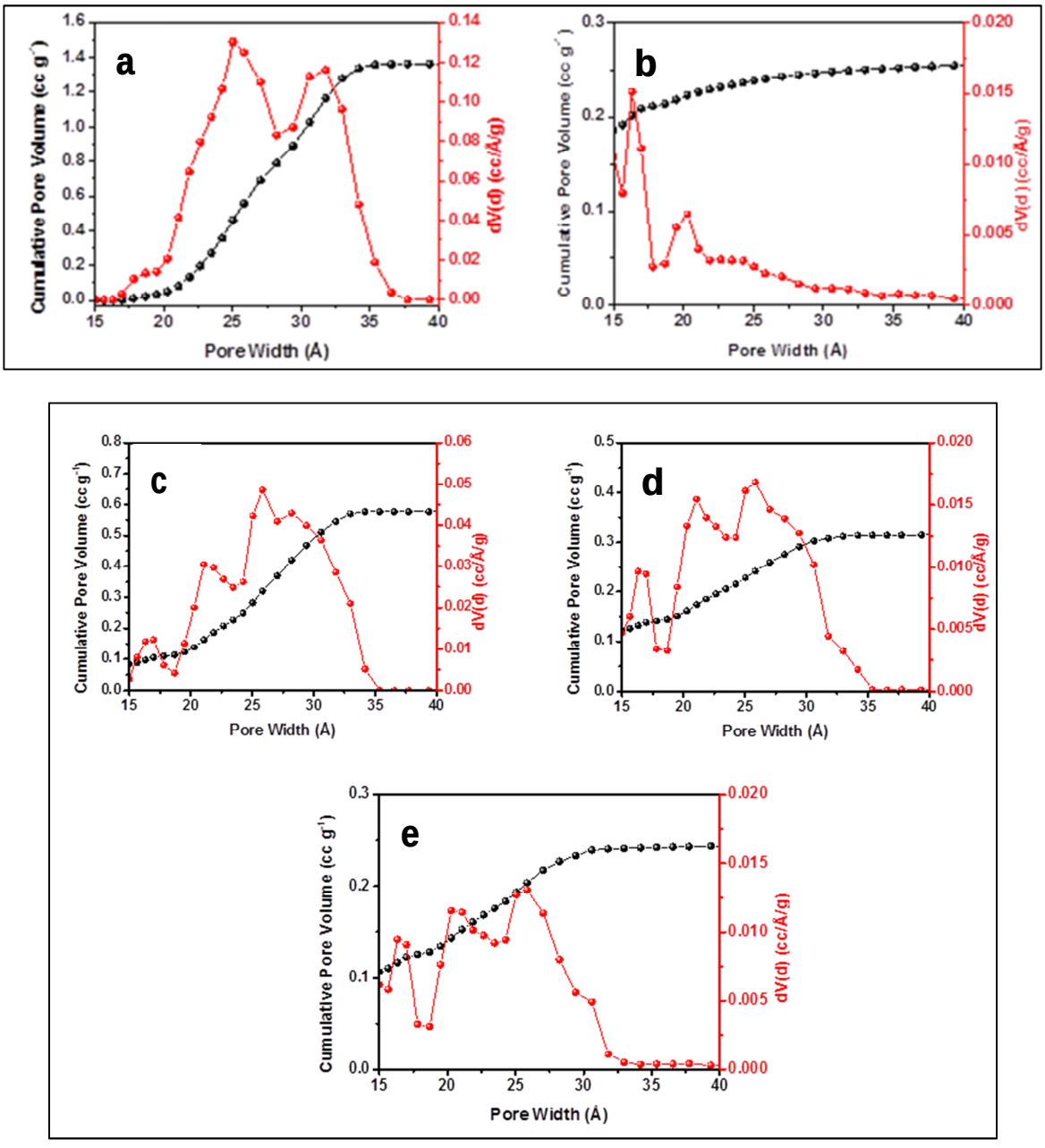

Figure S5. Pore distribution of MIL-101 activated at **a**) 200° **b**) 350°C, **c**) Fc@MIL-101 after 4h loading and activated at 200°C **d**) Fc@MIL-101 after 24h loading and activated at 200°C, and **e**) composite MIL-101

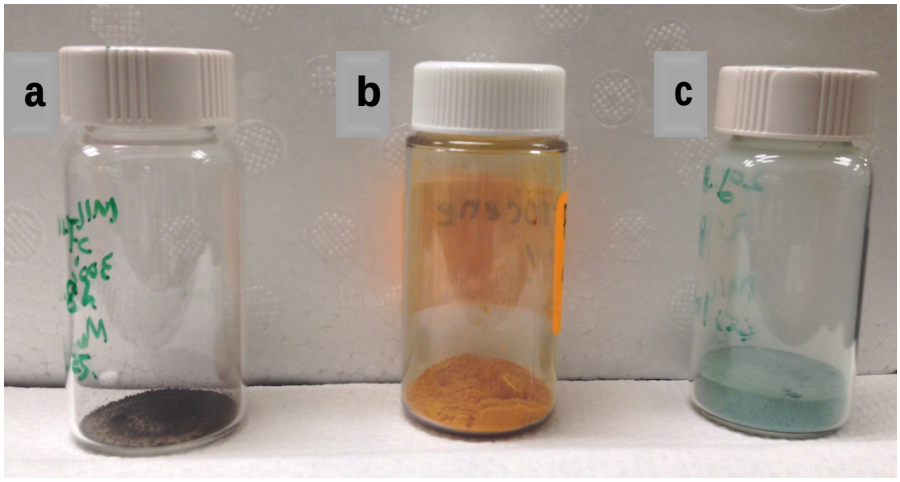

Figure S6. a) Fc@MIL-101 **b**) Ferrocene and **c**) MIL-101

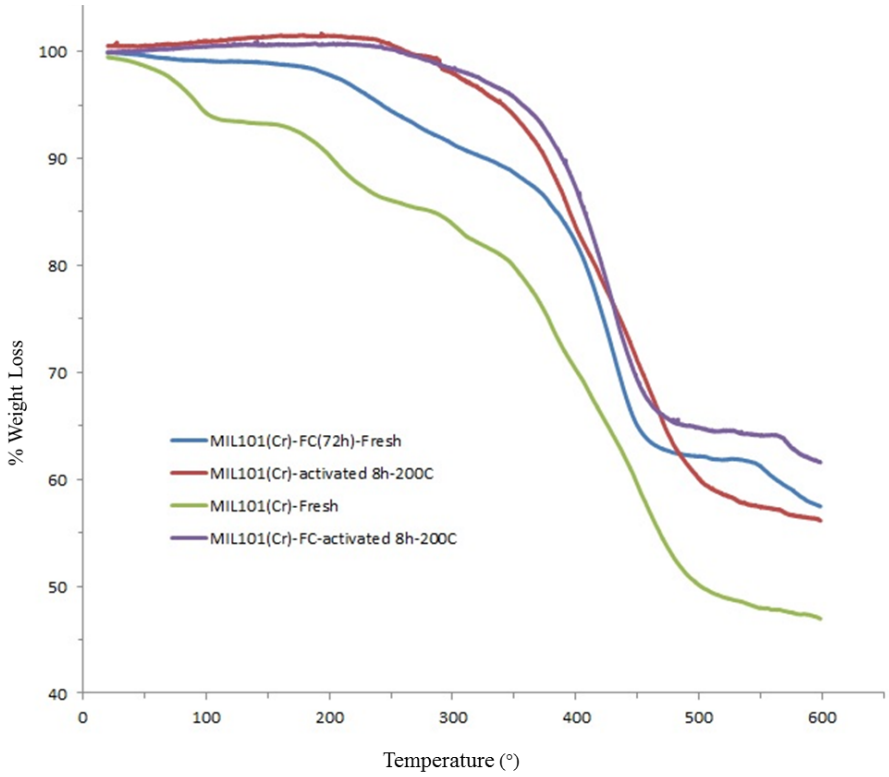

Figure S7. Thermogravimetric analyses of freshly synthesized MIL-101 (green), MIL-101 activated at 200°C 8h (red), Fc@MIL-101 (blue) and Fc@MIL-101 activated at 200°C 8h (purple).

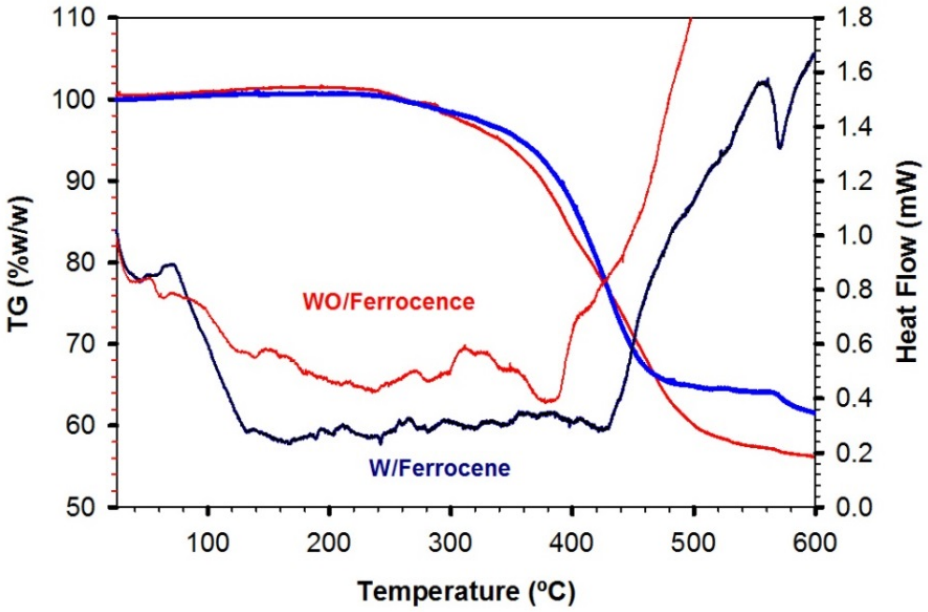

Figure S8. Thermogravimetric and differential scanning calorimetry analyses for evacuated MIL-101 (red) and Fc@MIL-101 (blue) after activated at 200°C 8h.

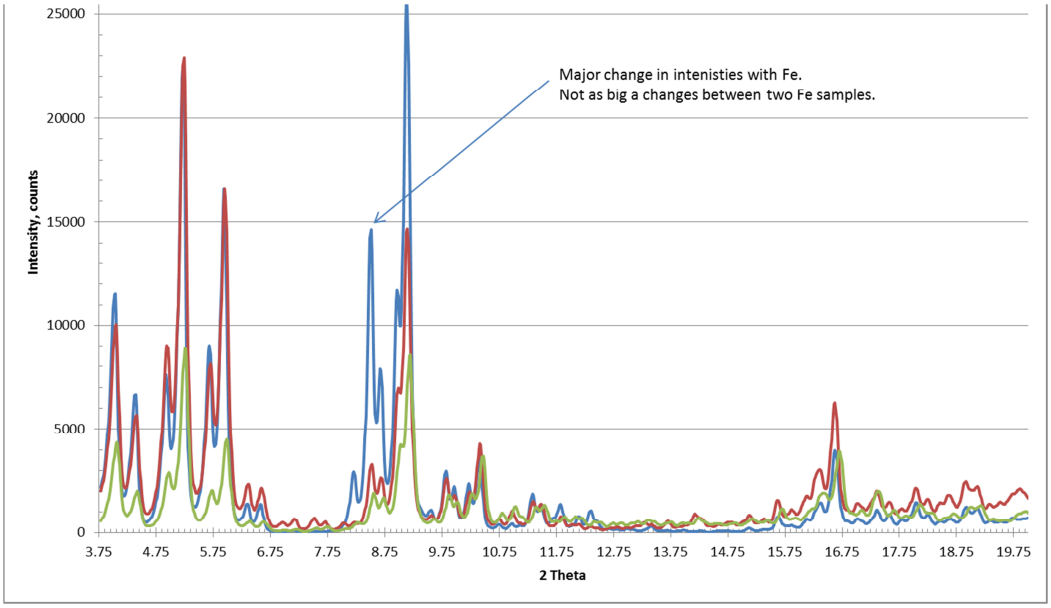

Figure S9. PXRD for MIL-101 (red), Fc@MIL-101 (green) and Fc@MIL-101 (blue) activated at 200 C for 12 h. The temperature dependent diffraction patterns of Fc@MIL-101 were fitted with Pawley Whole Pattern Decomposition model, which indicate that the cell parameters remains a good fit with pristine MIL-101 (unit cell dimension = 88.7

Vs 88.37 Å for MIL-101 and Fc@MIL-101) indicating no structural change upon Fc incorporation

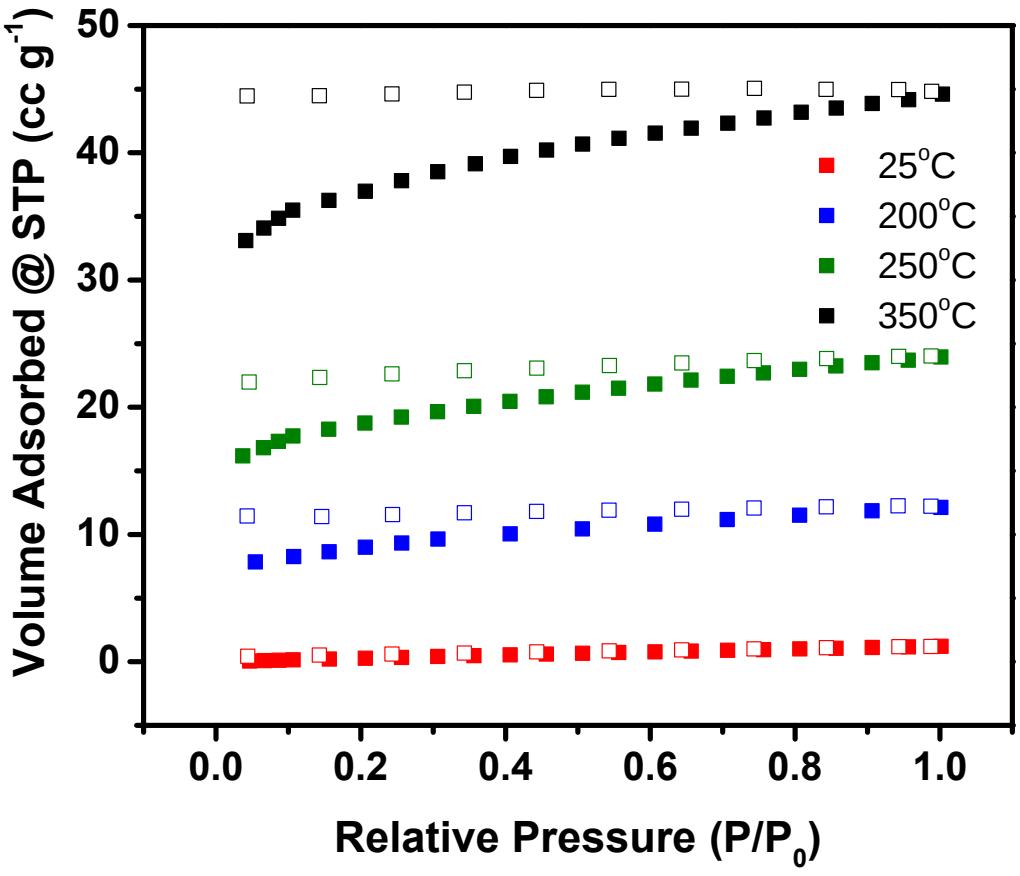

Figure S10 Oxygen adsorption-desorption isotherms at 298K for Fc@MIL-101 (loading for 72h), activated at different temperature (open symbol-desorption, closed symbol: adsorption)

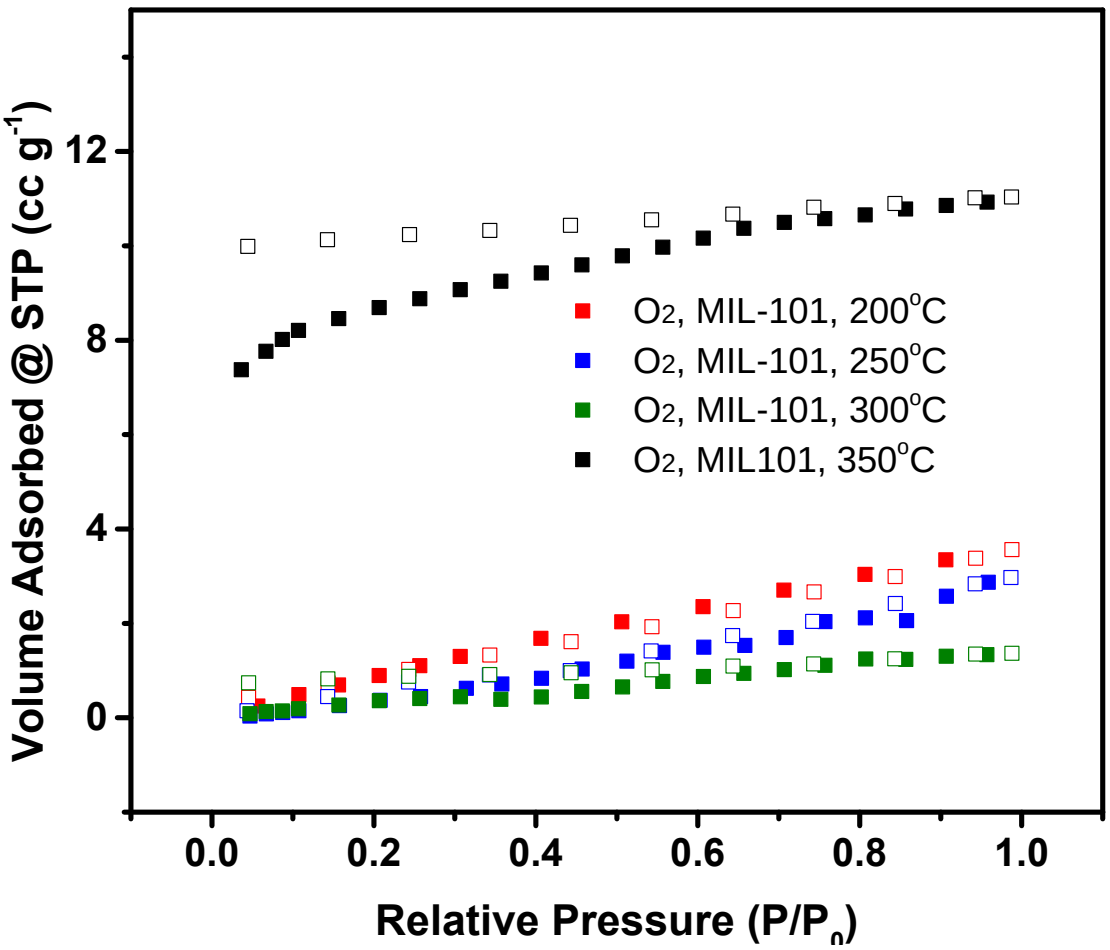

Figure S11. Oxygen adsorption-desorption isotherms at 298K for pure MIL-101 activated at 200 to 350°C (open symbol-desorption, closed symbol: adsorption)

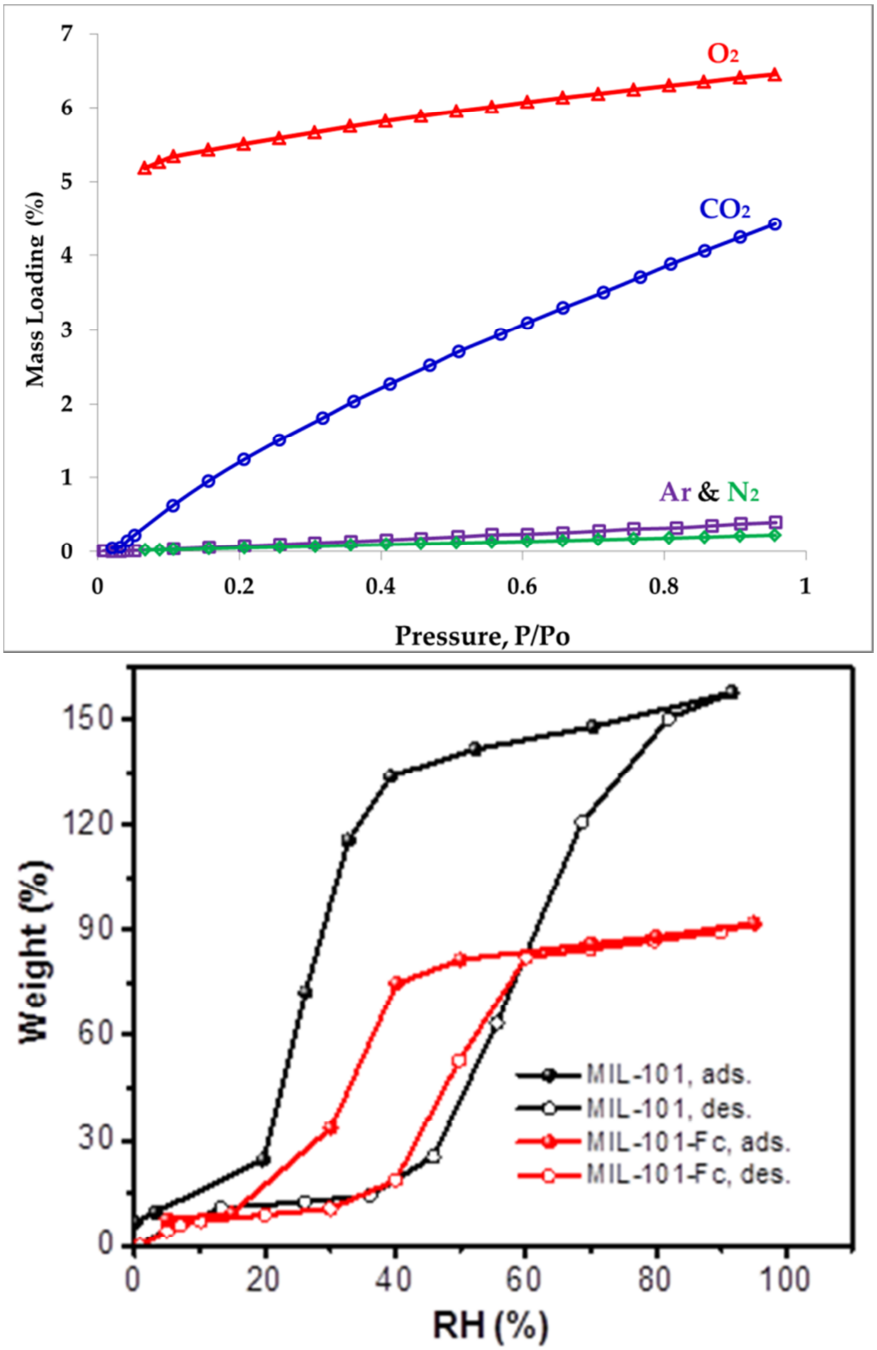

Figure S12. Oxygen, Nitrogen, Carbon dioxide and argon adsorption at room temperature in composite-MIL-101 activated at 350° C. Similarly, water adsorption in MIL-101 and Fc@MIL-101 (activated at 150° C) at RT.

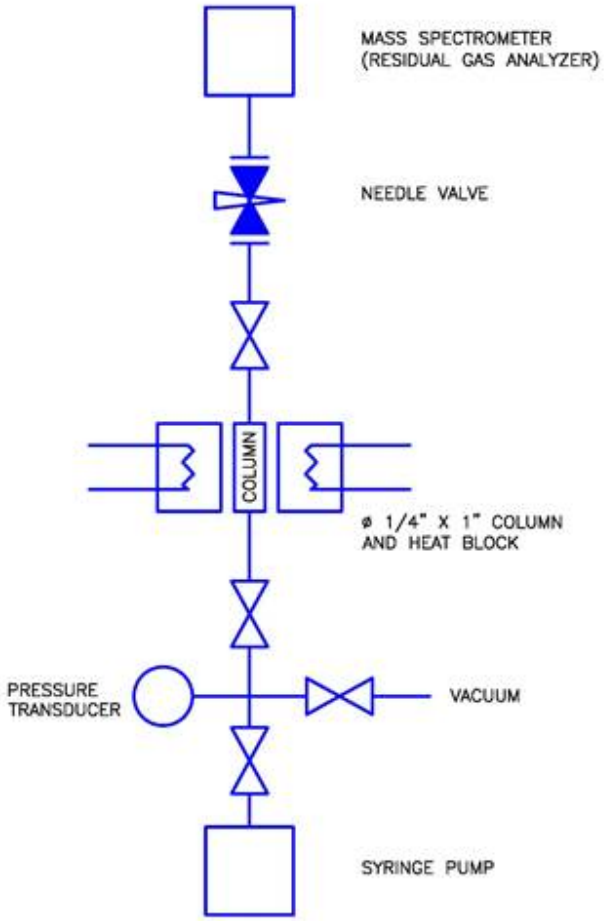

Figure S13. Schematic diagram of breakthrough analysis coupled with residual gas analyzer.

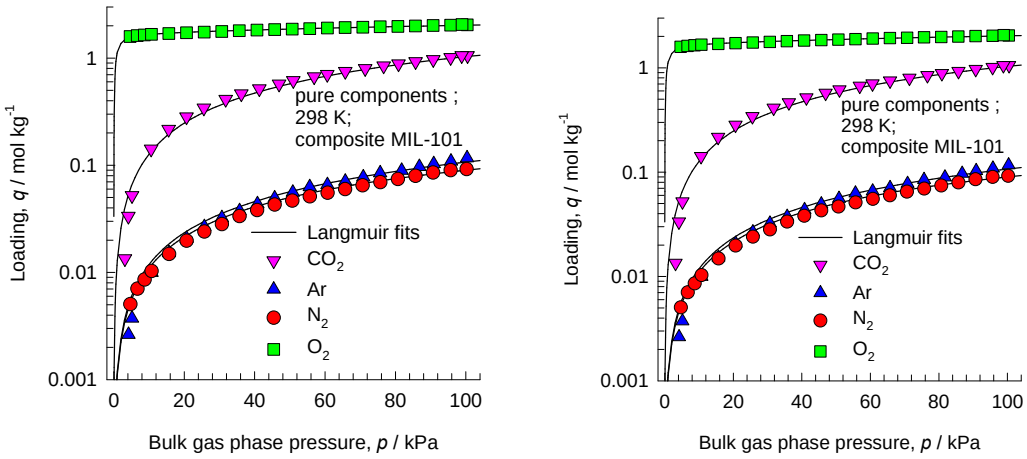

Figure S14. Comparison of experimental data on pure component loadings of O_2N_2, CO_2 and Ar in composite-MIL-101 at 298 K with Dual Langmuir fits using the parameters specified in Table S2.

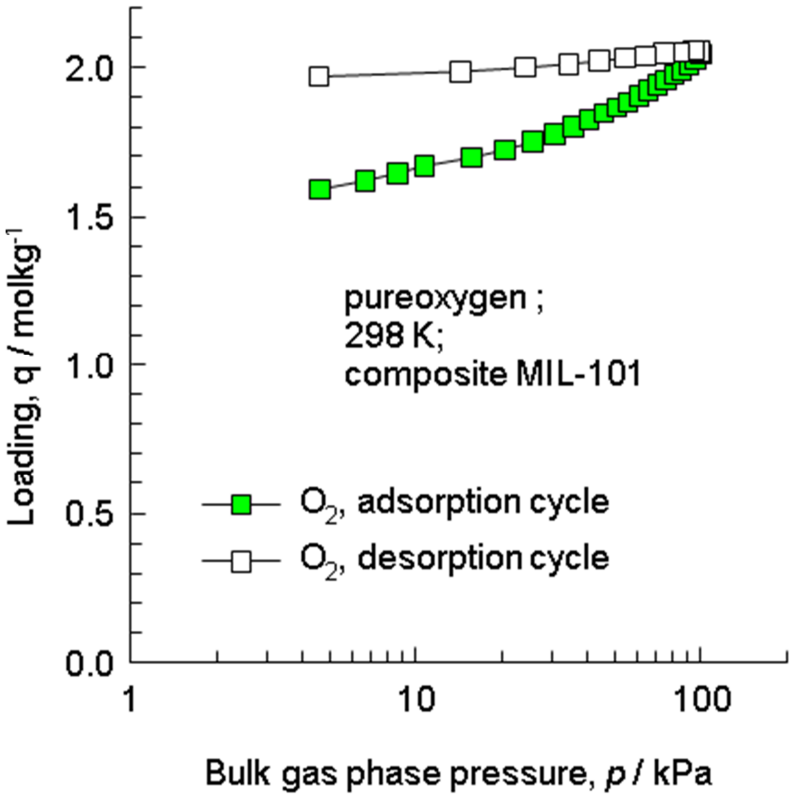

Figure S15. Adsorption – desorption cycles for O_2 in composite MIL-101 at 298 K.

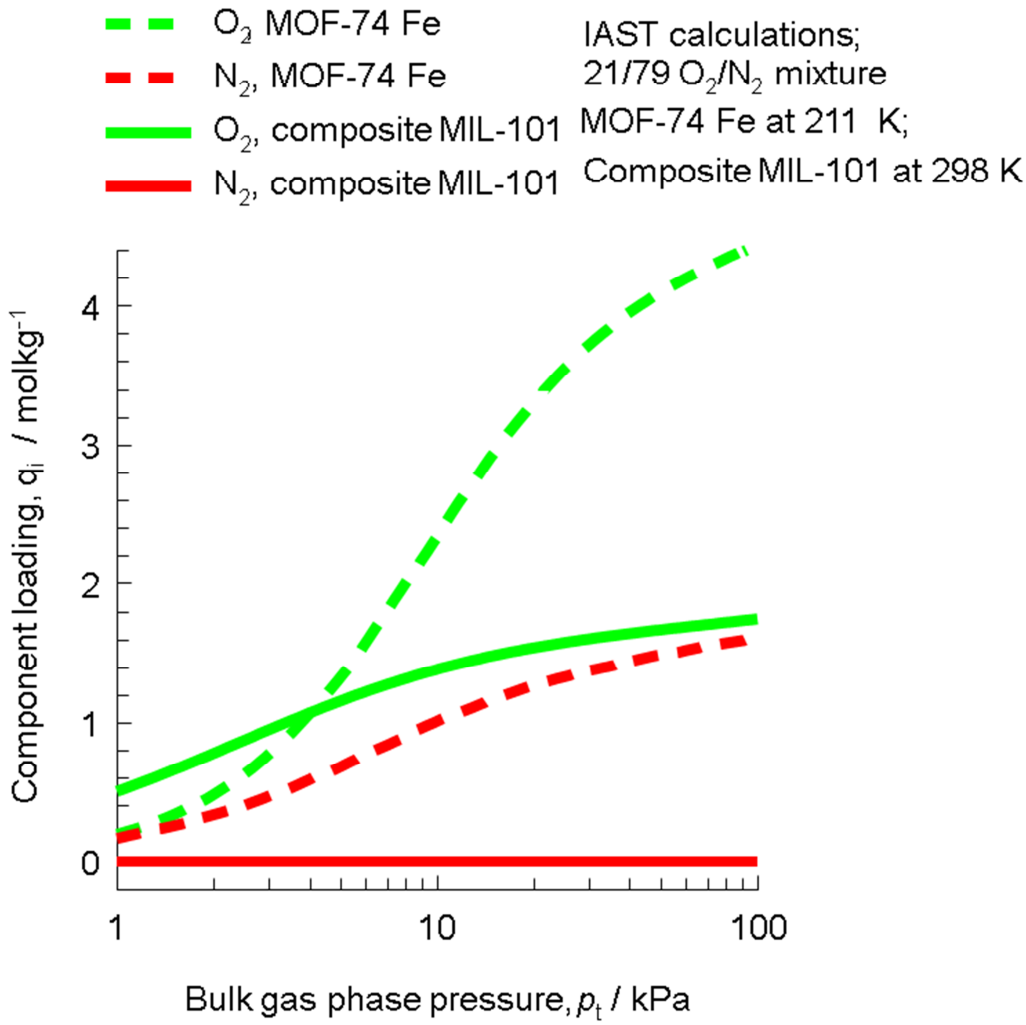

Figure S16. Calculations using the Ideal Adsorbed Solution Theory (IAST) for the component loadings of O_2, and N_2 in composite MIL-101 at 298 K in equilibrium with 21/79 O_2/N_2 mixtures at varying total gas phase pressures p_t. The dashed lines are the component loadings in MOF-74 Fe at 211 K.

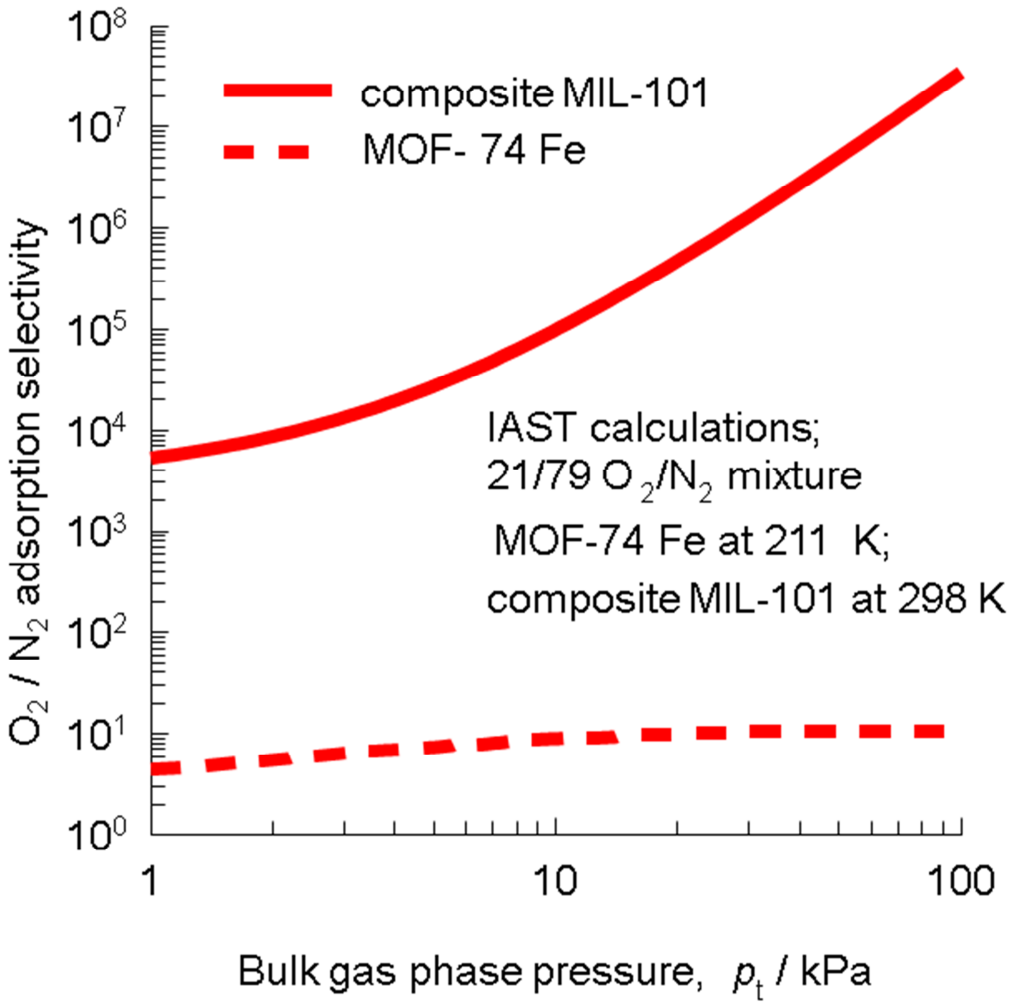

Figure S17. Calculations using the Ideal Adsorbed Solution Theory (IAST) for O_2/N_2 adsorption selectivity in composite MIL-101 at 298 K. The bulk gas phase contains 21/79 O_2/N_2 mixtures at varying total gas phase pressures p_t. The dashed lines are the component loadings in MOF-74 Fe at 211 K.

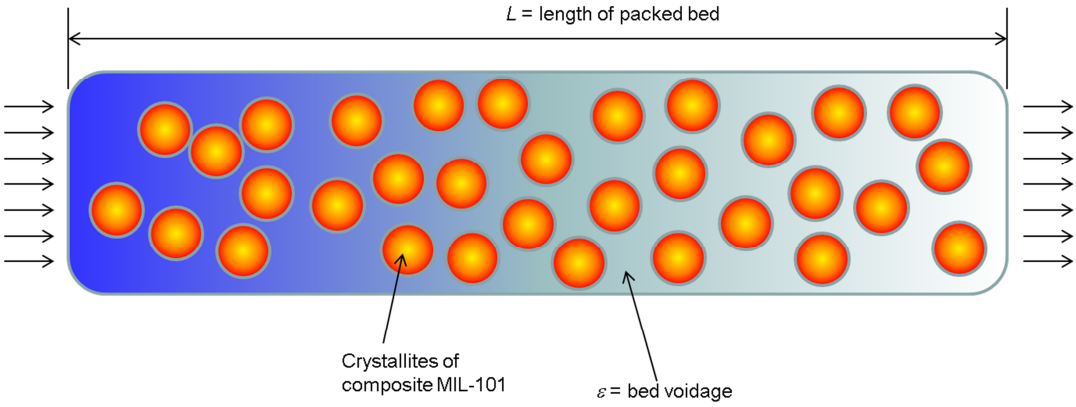

Figure S18. Schematic of a packed bed adsorber

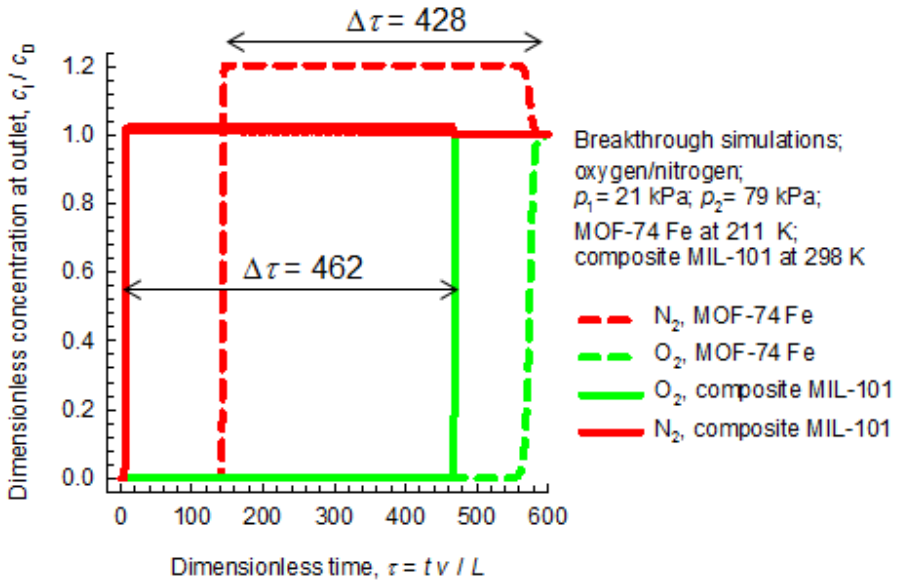

Figure S19. Transient O_2/N_2 breakthrough characteristics of fixed bed adsorber packed with composite MIL-101 and MOF-74 Fe operating at a total pressure of 100 kPa at 298 K (211 K for MOF-74 Fe. The partial pressures of the components in the bulk gas phase at the inlet are p_{O2}= 21 kPa, p_{N2} = 79 kPa. Other parameter values are: L = 0.3 m; voidage of bed, ε = 0.4; interstitial gas velocity, v= 0.1 m/s.

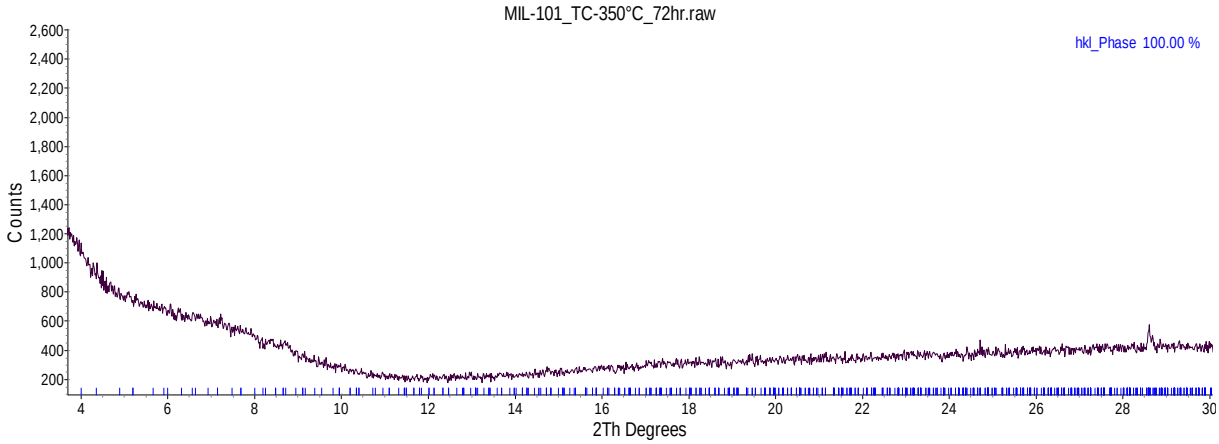

Figure S20. PXRD for composite-MIL-101 after 72 hours loading followed by activation at 350°C.

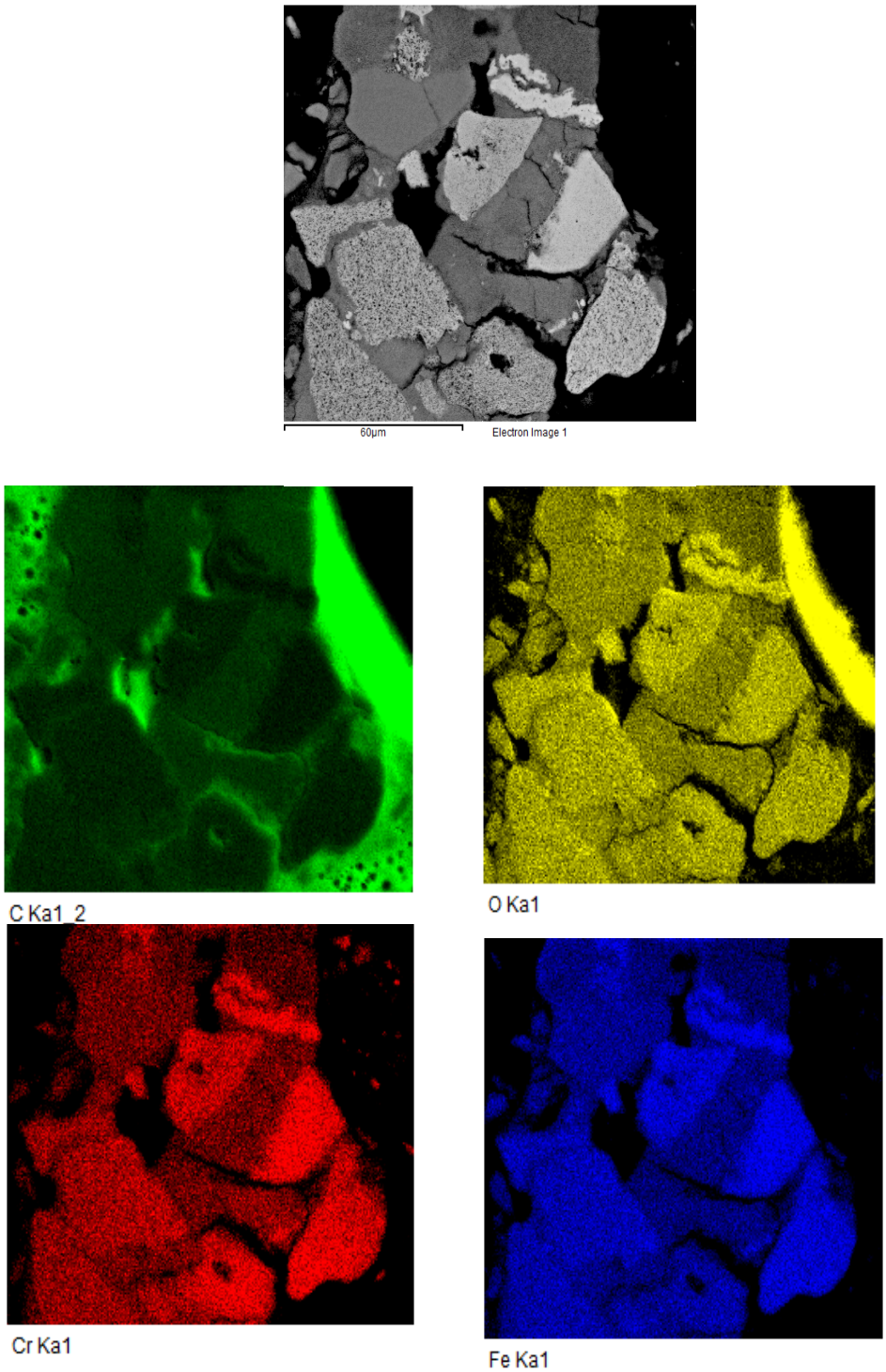

Figure S21. SEM images of composite-MIL-101 and the corresponding EDX mapping for C (green), O (yellow), Cr (red) and Fe (blue).

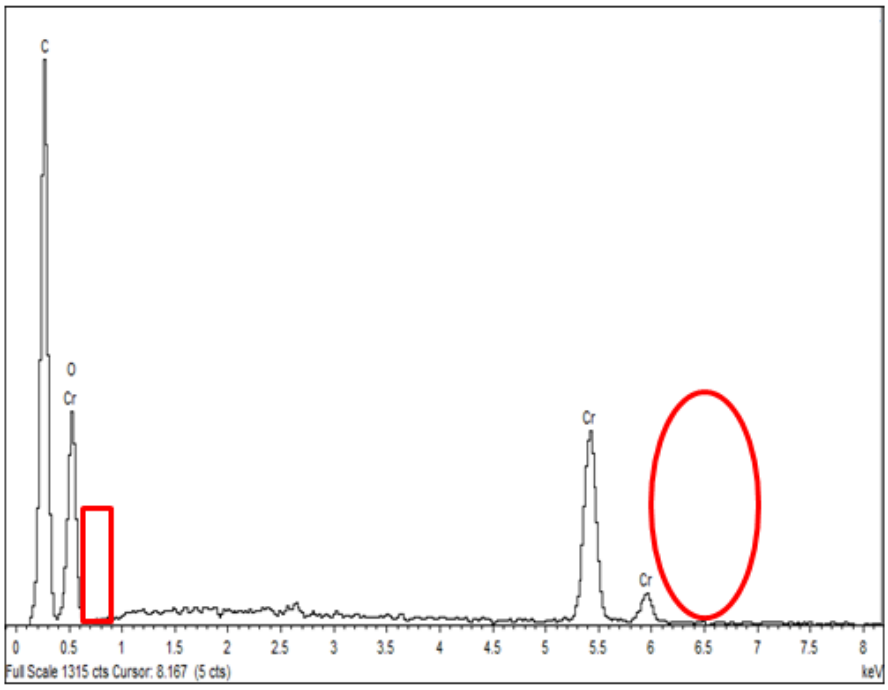

Figure S22. EDX data for MIL-101 (activated at 350°C)

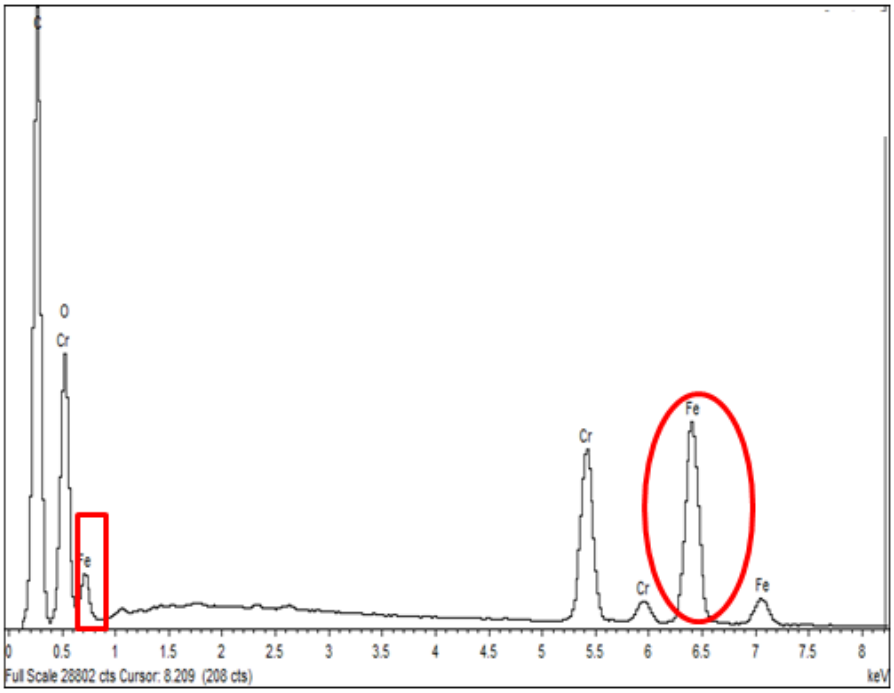

Figure S23 . EDX data for composite MIL-101

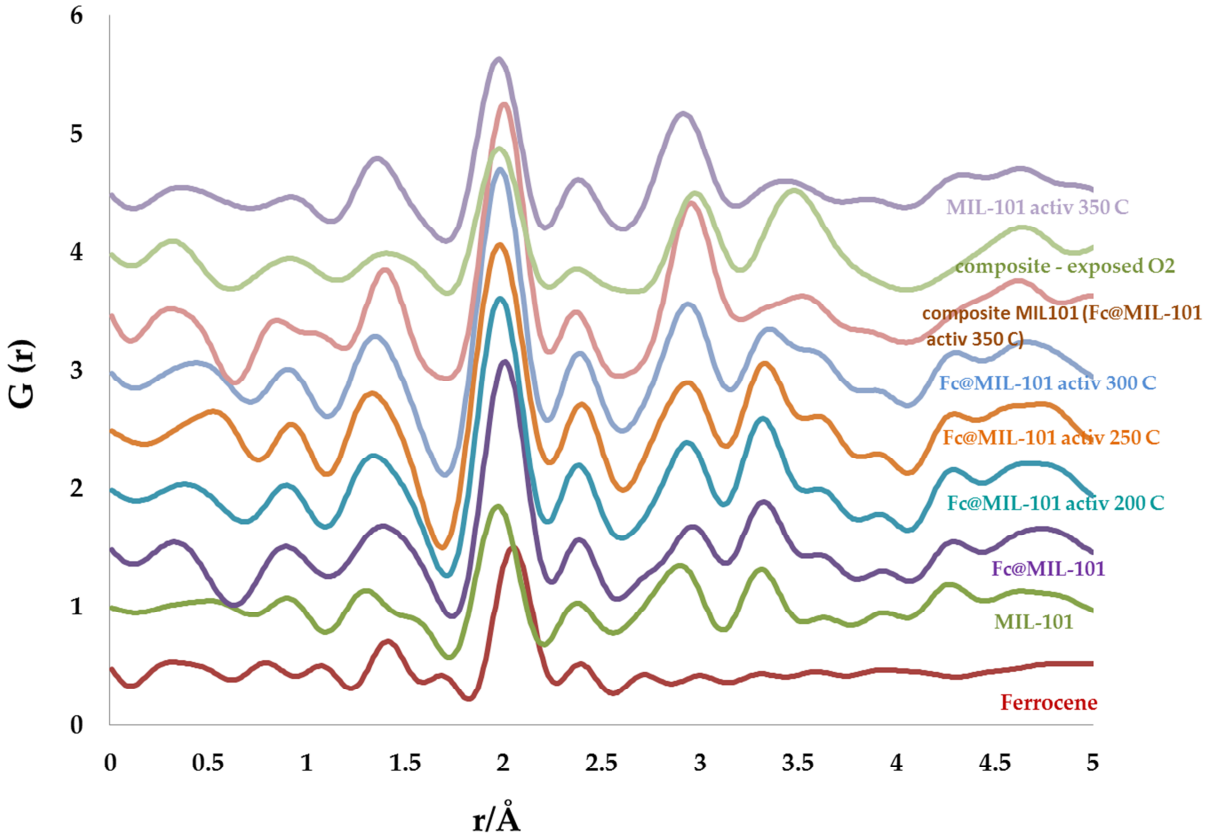

Figure S24. The PDF data for Fc@MIL-101 as a function of temperature

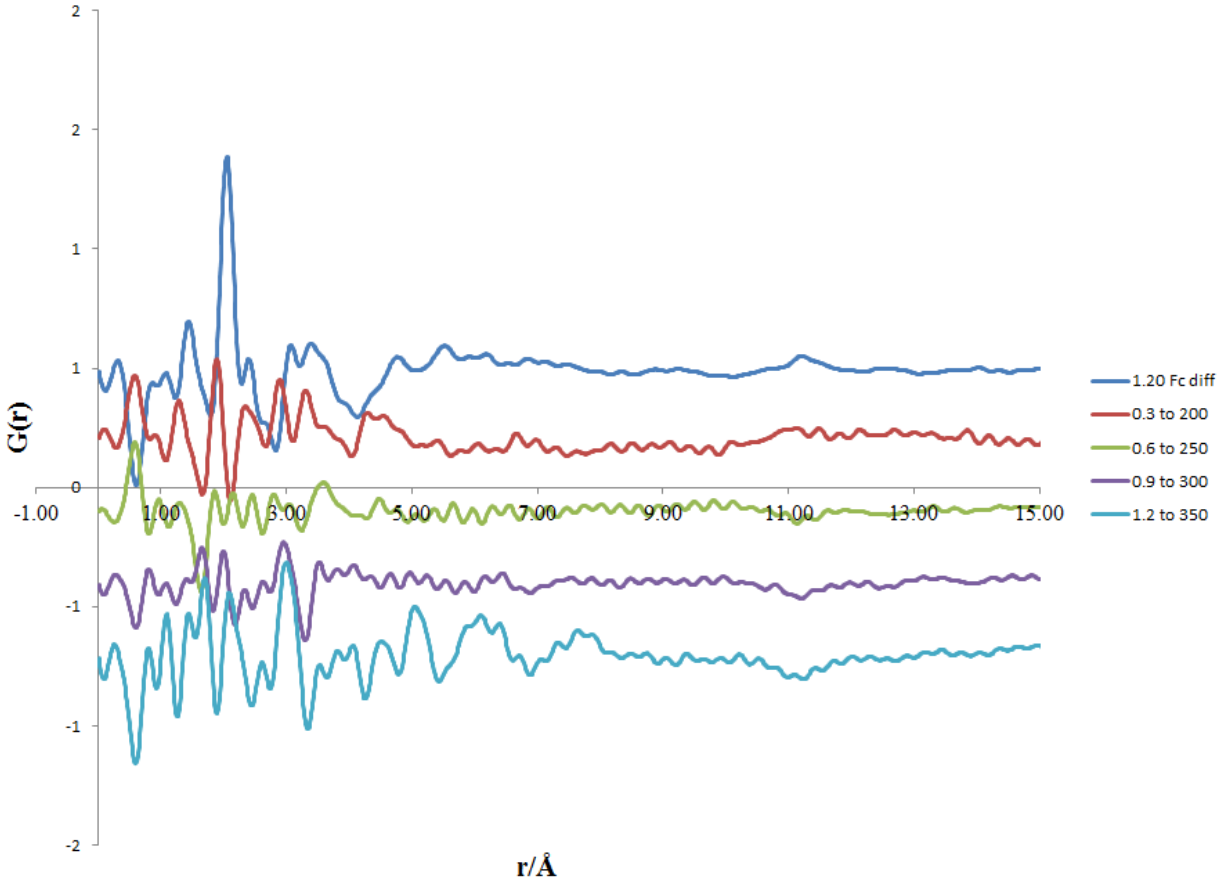

Figure S25. The difference PDF data for Fc@MIL-101

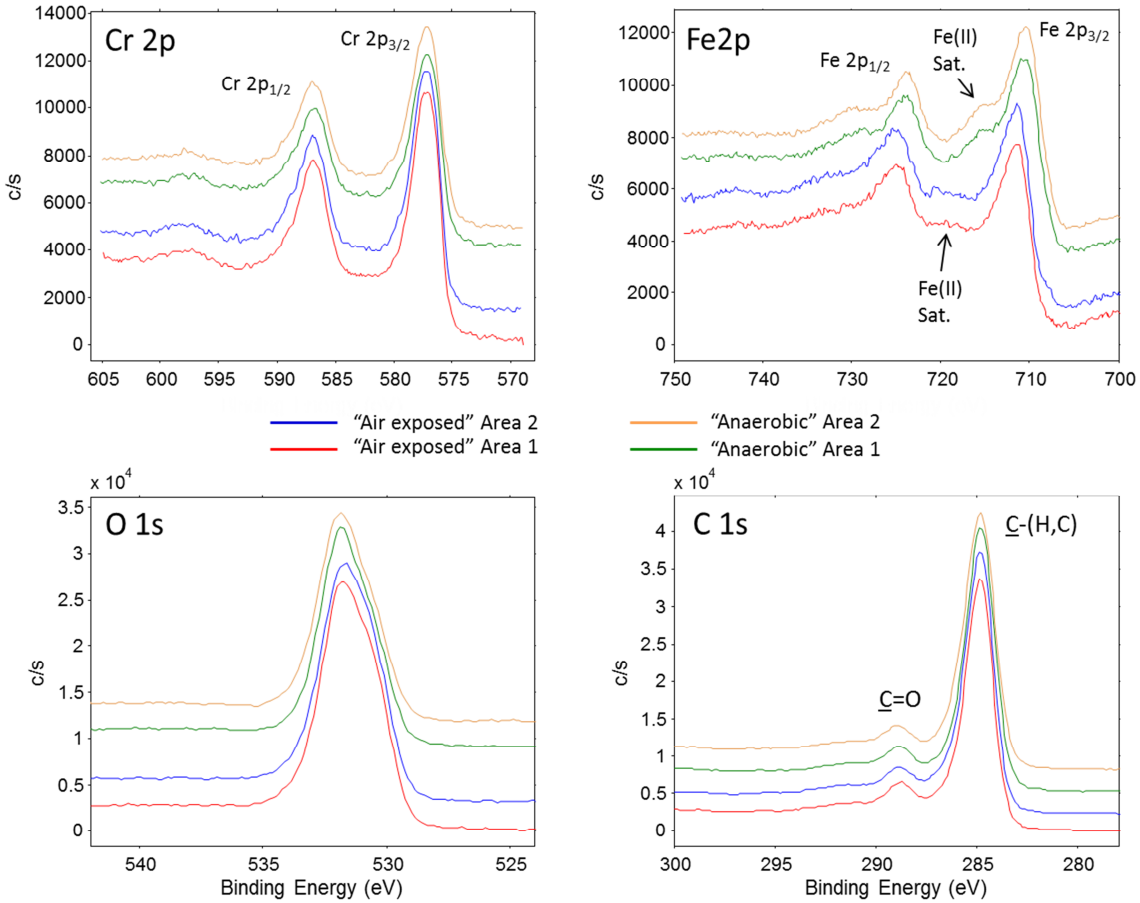

Figure S26. X-ray Photoelectron Spectroscopy (XPS) for the composite-MIL-101 (before and after O_2 adsorption)

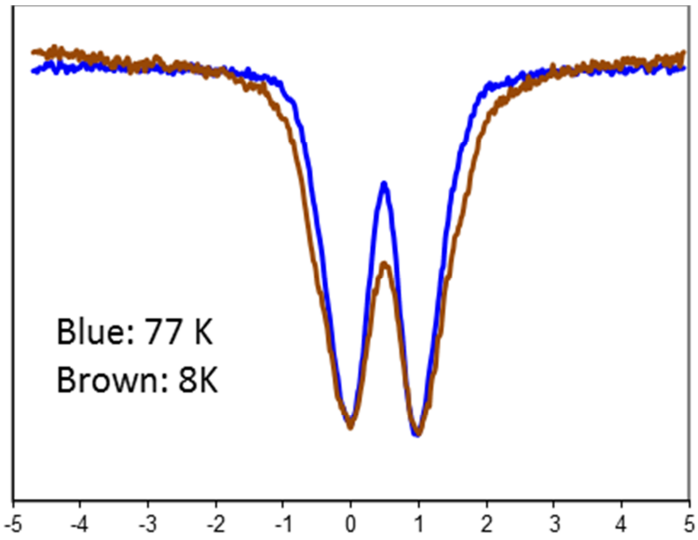

Figure S27. Mossbauer spectroscopy for composite MIL-101

Cycle study: Cycle study was performed activating the composite MIL-101 at 350 C after each adsorption cycle. The oxygen adsorption isotherm was collected at room temperature**.**

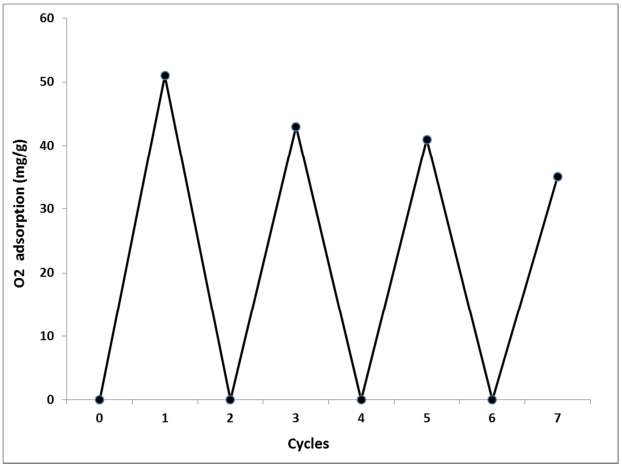

Figure S28. The O_2 adsorption-desorption cycle of composite MIL-101. After the first O_2 adsorption-desorption cycle the material was re-activated AT 150°C for 1 hour.

Table S1 Pore parameters calculated according to the N_2 adsorption isotherms at 77 K

Samples	Multiple BET Surface Area m^2/g	Langmuir Surface Area m^2/g	BJH Cumulative Adsorption Pore Volume cc/g
MIL-101	3083	4809	1.61
MIL-101-350 °C	658	846	0.325
Fc@MIL-101-RT	847	1424	0.664
Fc@MIL-101-200 °C	710	1160	0.501
Fc@MIL-101-250 °C	438	697	0.317
Fc@MIL-101-300 °C	273	441	0.264
composite MIL-101 (Fc@MIL-101-350 °C)	264	424	0.271

Table S2. Dual-site Langmuir parameter fits for O_2 and N_2 in composite MIL-101. The experimental isotherm data on excess loadings were converted to absolute loadings using the procedure described in detail in the Supporting Information accompanying the paper of Wu et al.[1] For this purpose, the pore volume of composite MIL-101 was taken to be 0.25 cm^3/g.

	Site A		Site B	
	$q_{A,sat}$ mol kg^{-1}	b_{A0} Pa^{-1}	$q_{B,sat}$ mol kg^{-1}	b_{B0} Pa^{-1}
O_2	1.7	2×10^{-3}	2	2×10^{-6}
N_2	0.45	2×10^{-6}		
CO_2	5	2.6×10^{-6}		
Ar	1	1.2×10^{-6}		

Table S3 Average Element ratio from EDX

All results in atom%

Samples	C	O	Cr	Fe	Total
MIL-101-200 °C	77.71	19.68	2.61	0	100
MIL-101-350 °C	66.07	29.60	4.33	0	100
Fc@MIL-101-200 °C	69.02	23.82	5.24	1.92	100
Fc@MIL-101-300 °C	65.59	28.00	2.61	3.80	100
Composite MIL-101 (Fc@MIL-101-350 °C)	68.82	24.51	2.66	4.01	100

Table S4: RT Modeled Mossbauer spectral parameters

Sextet	<CS>[1] mm/sec	<QS>[2] mm/sec	σ_{QSD}[3] mm/sec	area %[4]
Ferrocene	0.44	2.38	0.09	100
Composite MIL-101 *Ferrocene*	0.42	2.12	0.3	6

Fe^{2+}-HS a	1.02	1.77	0.55	75
Fe^{2+}-HS b	0.62	1.03	0.4	20
Composite MIL-101 + O_2				
Ferrocene	0.41	2.12	0.3	7
"Maghemite"	0.37	1.06	0.45	93

[1] center shift; [2] quadrupole splitting; [3] QS standard deviation; [4] relative spectral area

Lorentzian half-width at half maximum is fixed at 0.097 mm/sec.

Spectra were modeled using Voigt-based method of Rancout and Ping (1991)

(Voigt-based methods for arbitrary-shape static hyperfine parameter distributions in

Mossbauer Spectroscopy: Nuclear Instrumentation Methods in Physical Research B: 58, 85-97).

[1] H. Wu, K. Yao, Y. Zhu, B. Li, Z. Shi, R. Krishna, J. Li, *J. Phys. Chem. C* **2012**, *116*, 16609-16618.